Fermi National Accelerator Laboratory

FERMILAB-Pub-88/74-A
June 1988

Cross Sections, Relic Abundance, and Detection Rates for Neutralino Dark Matter

KIM GRIEST

Astronomy and Astrophysics Center, Enrico Fermi Institute, The University of Chicago, Chicago, Illinois 60637

and

NASA/Fermilab Astrophysics Center, Fermi National Accelerator Laboratory, Batavia, Illinois 60510

Operated by Universities Research Association Inc. under contract with the United States Department of Energy

ABSTRACT

Neutralino annihilation and elastic scattering cross sections are derived which differ in important ways from previous work. These are applied to relic abundance calculations and to direct detection of neutralino dark matter from the galactic halo. Assuming the neutralino is the lightest supersymmetric particle and that it is less massive than the Z^0, we find relic densities of neutralinos greater than 4% of critical density for almost all values of the supersymmetric parameters. We constrain the parameter space by using results from PETRA (chargino mass less than 23 GeV) and ASP, and then assuming a critical density of neutralinos, display event rates in a cryogenic detector for a variety of models. A new term implies "spin independent" elastic scattering even for these majorana particles and inclusion of propagator momenta increases detection rates by 10% to 300% even for pure photinos. Z^0-squark interference leads to very low detection rates for some values of the parameters. The new term in the elastic cross section dominates for heavy, mostly spinless materials and mitigates the negative interference cancellations in light materials; except for the pure photino or pure higgsinos cases where it does not contribute. In general, the rates can be substantially different from the pure photino and pure higgsino special cases usually considered.

I. Introduction

One of the most interesting unsolved problems in physics today is the identity of the dark matter (DM) known to exist in galactic halos. Several lines of reasoning lead one to hypothesis that the DM may not be ordinary "baryonic" material but rather may consist of some, as yet undiscovered, elementary particle. If so, it is likely that substantial quantities of these particles exist in our galaxy's halo at the position of the Earth and it may be possible to detect these particles as they pass through detectors in laboratories on Earth.[1-4] Indirect methods, such as detecting the products of DM particle-antiparticle annihilation have also been suggested, the most promising of which use the enhancement in density which results from capture of DM particles into the body of the Sun or Earth.[5,6]

Crucial to all detection schemes are the DM particle cross sections. A zero elastic scattering cross section off ordinary matter would mean no possibility of direct direction and no capture of particles into the Earth or Sun. Particle-antiparticle annihilation cross sections determine, in part, the relic abundance of DM particles and also the flux of detectable annihilation products. Since there is little astrophysical data which bear on these cross sections we must turn to particle physics models to make predictions. A wide spectrum of candidate particles have been proposed, but the most interesting are those which were originally proposed for non-astrophysical reasons, and only subsequently turned out to be suitable as DM candidates. The most popular particles in this class are the neutrino, the axion, and the lightest supersymmetric particle (LSP). In this Report we consider only the LSP.

Supersymmetry has been immensely popular among theorists for the past decade. It seems to be an essential ingredient of theories which unify gravity with the other interactions and in its low-energy manifestation provides an elegant solution to the hierarchy problem.[7] Supersymmetry has also been popular among experimentalists, but although much effort has been expended in the

search, no supersymmetric particles have been discovered. A major goal of the next generation of particle accelerators will be to discover or set limits on supersymmetric particles. In the minimal supersymmetric extension of the Standard Model which we consider here, there is a new fermionic (bosonic) superpartner for every bosonic (fermionic) ordinary particle, so there is a doubling of the number of Standard Model particles. The masses of these particles are undetermined in the most general scheme, but if supersymmetry is to solve the hierarchy problem, some superpartners must exist with masses below roughly a TeV. In most versions of these models there is also a conserved multiplicative quantum number $R = -1^{2S+3B+L}$. This R-parity implies that the lightest superpartner is stable and therefore a DM candidate. The identity and cosmology of the LSP was considered in 1984 by Ellis *et al.*,[9] and since then, the lightest neutralino ($\tilde{\chi}$), a linear combination of the photino, zino and two neutral higgsinos, has been considered the likely candidate for LSP.[10] In considering detectability, most authors have, however, considered only the pure photino and pure higgsino, two special cases of the general neutralino. If the neutralino is very light, then one might expect a reasonably pure photino or higgsino, but there are no strong theoretical or experimental reasons to expect such a light LSP, and as the mass of the neutralino increases, a pure photino or higgsino becomes more and more unlikely.

One of the most remarkable characteristics of neutralinos is that over most of the supersymmetric parameter space a relic density $\rho_{\tilde{\chi}}$ near critical density is obtained. We emphasize that a value of $\Omega_{\tilde{\chi}}$ (defined as $\rho_{\tilde{\chi}}/\rho_{crit}$) near 1, is therefore very natural, and this fact adds motivation to the search for neutralino dark matter (See also Ref. 9). In fact, even if neutralinos do not constitute the DM responsible for galactic rotation curves, we still expect $\Omega_{\tilde{\chi}} \geq .04$ in our galactic halo as long as they exist and are the LSP. So if low-energy supersymmetry does exist we expect to find a substantial fraction of the mass of the universe in neutralinos and it is therefore worth making the effort to detect them.

In this Report we recalculate the cross sections for neutralinos and find several important differences with respect to earlier work.[9] Using these cross sections we show that direct detection event rates in cryogenic detectors can be very different from the pure photino and pure higgsinos special cases. We also find

that as the neutralino becomes more massive pure photinos and especially pure higgsinos become very unlikely. Including a new term in the elastic scattering cross section and using a method due to Shifman *et al.*,[11] which includes the effects of heavy quark loops, we find a piece of the elastic cross section which is proportional to the mass of the scattering nucleus. This means neutralinos might be detectable with mostly spinless material such as mercury, germanium or helium, even though majorana particles are usually thought to have only "spin dependent" interactions.

Inclusion of several new terms in the annihilation cross section, as well as a different sign interference term, changes relic abundance results for neutralinos, and the inclusion of previously ignored effects such as propagator momenta changes the results even for pure photinos. Finally, since the same couplings are involved in the elastic, annihilation, and production cross sections[12] we can extract information from various accelerator experiments. In particular, large areas of neutralino parameter space are ruled out by experiments such as UA1,[13] PETRA,[14] and ASP,[15] and we find that neutralinos with mass less than about 5 GeV are unlikely.

The plan of this Report is as follows. In Sec. II we define the models under consideration and the parameter space to be explored. We then calculate the $\bar{\tilde{\chi}}\tilde{\chi}\bar{q}q$ matrix element (q is any quark or lepton) and the annihilation cross section ($\bar{\tilde{\chi}}\tilde{\chi} \to \bar{q}q$). For use in relic abundance calculations we also present the non-relativistic expansion including the possibly important effect of propagator momenta. Exploiting crossing symmetry, we use the annihilation matrix element to find the elastic scattering ($\tilde{\chi}q \to \tilde{\chi}q$) and production ($e^+e^- \to \bar{\tilde{\chi}}\tilde{\chi}$) cross sections. For use in comparison with ASP results, we finally present the cross section $\sigma(e^+e^- \to \bar{\tilde{\chi}}\tilde{\chi}\gamma)$ in the soft photon limit.

In Sec. III we re-derive and extend some of the results from Sec. II using an effective Lagrangian approach. In particular, we find the elastic scattering cross section of neutralinos off nuclei rather than neutralinos off quarks and show that due to heavy quark loops, a "spin independent" interaction exists for the general neutralino. This interaction is proportional to the zino component and so does not contribute to pure photino or pure higgsino scattering. We also point out a

difference (with respect to earlier work) of the sign of an interference term.

In Sec. IV we use the annihilation cross section to calculate the relic abundance of neutralinos and show that $\Omega_{\tilde{\chi}} \sim 1$ is very natural. We also show that apart from near the Z^0 pole a very low relic density of neutralinos is unlikely. We also describe and implement several consistency requirements such as the neutralino being lighter than the squarks and the charginos.

In Sec. V we use the elastic cross section to find the rate at which DM neutralinos interact with nuclei in a cryogenic detector. We show that the new (scalar) term can give enhancements of several orders of magnitude for very heavy nuclei. We also point out that with the standard "spin dependent" (axial vector) cross section very low event rates generically occur due to negative interference between Z^0 and squark exchange. These cancellations are substantially mitigated by the new scalar term even for light elements. We reduce parameter space throughout by requiring that $\Omega_{\tilde{\chi}} = 1$. We also mention that the inclusion of propagator momenta can be important, especially when the neutralino mass nears the squark mass. This is illustrated for the pure photino case where, for a neutralino mass of 30 GeV, the event rate with propagator momenta included is a factor of two higher than without. We emphasize that the event rates for the general neutralino can be quite different from the pure photino and pure higgsino special cases, and that since detection should be aimed at the general neutralino, all terms in the cross section should be taken into account when selecting detector material.

In Sec. VI we show how accelerator experiments can compliment dark matter searches. In particular, the PETRA result[14] that $m_{\tilde{\chi}^{\pm}} < 23$ GeV eliminates large regions of parameter space and as these limits improve (or the chargino is detected) the chargino constraint will be come more and more important in deciding the detectability of neutralino DM. In addition, the ASP limit[15] $\sigma(e^+e^- \to \gamma + \text{missing}) < .03$ pb is re-examined for the case where "missing" is a pair of neutralinos, and again parts of parameter space are eliminated. While the PETRA constraint eliminates mostly states with a substantial zino component, the ASP constraint rules out light, mostly photino states, and together the constraints rule out almost all states with mass less than about 5 GeV.

Finally, in Sec. VII we consider the effect of relaxing several simplifying assumptions made during the first six sections. We consider the effect the new EMC spin dependent structure functions[16] have on direct detection, and find a sensitivity to the composition of the neutralino and shell model parameterization of the nuclei whenever the axial vector term dominates the elastic cross section. For shell model "neutrons" there is a general lowering of rates, except for photino-like states which are greatly enhanced. The change in rates for shell model "protons" is not as large except again for photino-like states which are somewhat suppressed. However, while details can vary substantially, the general picture remains unchanged. We also consider the effect of non-degenerate selectron and squark masses ($M_{\tilde{l}}$ and $M_{\tilde{q}}$ respectively). We show results for $M_{\tilde{q}} = 3M_{\tilde{l}}$ which, along with the previously considered $M_{\tilde{q}} = M_{\tilde{l}}$, bracket most of the models we surveyed from the literature. Event rates are in general one or two orders of magnitude lower, since annihilation through the slepton channels ($\propto M_{\tilde{l}}^{-4}$) can be strong, resulting in weaker couplings to achieve $\Omega_{\tilde{\chi}} = 1$, and these weaker couplings remain for the elastic scattering which proceeds via the heavier squark ($\propto M_{\tilde{q}}^{-4}$) exchange. Sec. VIII sums up the Report.

II. Cross sections

In this section we calculate the matrix element and cross section for the annihilation ($\bar{\tilde{\chi}}\tilde{\chi} \to \bar{q}q$) of two neutralinos into a fermion and antifermion, and then use crossing symmetry to find the elastic scattering ($\tilde{\chi}q \to \tilde{\chi}q$) and the anomalous single photon (ASP) ($e^+e^- \to \bar{\tilde{\chi}}\tilde{\chi}\gamma$) cross sections. Here q stands for any quark or lepton and e^- is the electron.

Throughout we will use the minimal supersymmetric extension of the Standard Model as described in Ref. 7 (see especially the appendices) and Ref. 8. This is a group of models which is minimal, in the sense that it contains the minimum number of new particles, and general, in the sense that it has all possible CP-conserving soft supersymmetry breaking terms included in the Lagrangian. In these models there exist four neutralinos which are linear combinations of the supersymmetric partners of the neutral W, the B, and the two neutral Higgs

bosons. These can also be characterized as the photino, zino and two neutral higgsinos. Only the lightest will be stable (we assume a conserved R parity and also that the lightest neutralino is the LSP) and we denote it as

$$\widetilde{\chi} = Z_{11}\widetilde{B} + Z_{12}\widetilde{W}^3 + Z_{13}\widetilde{H}_1 + Z_{14}\widetilde{H}_2, \tag{1}$$

where the Z_{1i} are the elements of the real orthogonal matrix which diagonalizes the neutralino mass matrix; that is, if $Z_{11} = Z_{12} = 0$, $\widetilde{\chi}$ is a pure higgsino, if $Z_{11} = \cos\theta_w, Z_{12} = \sin\theta_w$, $\widetilde{\chi}$ is a pure photino, and if $Z_{11} = -\sin\theta_w, Z_{12} = \cos\theta_w$, $\widetilde{\chi}$ is a pure zino. The assumption of CP-conservation ensures that the Z_{ij} are real.

The neutralino masses and the Z_{ij}'s are fully determined by four parameters: $\tan\beta$, μ, M, and M', where $\tan\beta = v_2/v_1$ is the ratio of Higgs vacuum expectation values,[17] M and M' are soft supersymmetry breaking parameters, and μ is a supersymmetric Higgs mass. Throughout, we make the standard[7] simplification $M' = \frac{5}{3}M\tan^2\theta_w$ which is true if the theory is eventually embedded in any simple grand unified group. Overall then we have three undetermined parameters: $\tan\beta$, M, and μ, and it is this parameter space we explore. We consider several representative values of $\tan\beta$ and M and μ in the wide range $0 \leq M, \mu \leq 1$ TeV.

For a neutralino of mass m_X less than the Z^0 mass m_Z, the annihilation, elastic scattering, and production ($e^+e^- \rightarrow \bar{\widetilde{\chi}}\widetilde{\chi}$) processes are all given by the five Feynman diagrams shown in Figure 1. There are four squark (or slepton) exchange diagrams and one Z^0 exchange. The Feynman rule for the left chiral $\widetilde{\chi}q\widetilde{q_L}$ vertex is $-ig\sqrt{2}(a\epsilon P_R + bP_L)$ and the rule for the right chiral $\widetilde{\chi}q\widetilde{q_R}$ vertex is $-ig\sqrt{2}(aP_L - \epsilon cP_R)$ where g is the electroweak coupling constant, $P_R = \frac{1}{2}(1+\gamma_5)$, etc. and

$$\begin{aligned} a &= m_q d_q/(2m_W) \\ b &= T_{3L}Z_{j2} - \tan\theta_w(T_{3L} - e_q)Z_{j1} \\ c &= \tan\theta_w e_q Z_{j1}. \end{aligned} \tag{2}$$

Here $d_q = Z_{j3}/\cos\beta$ for down type quarks or leptons and $d_q = Z_{j4}/\sin\beta$ for up types, m_q is the mass of the quark or lepton, T_{3L} is the weak isospin, e_q is the

charge, $\sin^2\theta_w = .23$, and ϵ is the sign of the neutralino mass eigenvalue. The "a" factor corresponds to a higgsino type coupling, while the "b" and "c" factors are the photino-zino couplings. The $Z^0\tilde{\chi}\bar{\tilde{\chi}}$ Feynman rule is $(ig/2\cos\theta_w)(Z_{13}^2 - Z_{14}^2)\gamma^\mu\gamma_5$ and the $Z^0 q\bar{q}$ rule is as usual $(-ig/\cos\theta_w)\gamma^\mu(c_L P_L + c_R P_R)$. Here $c_L = T_{3L} - e_q \sin^2\theta_w$ and $c_R = -e_q \sin^2\theta_w$. More details on the Feynman rules and techniques for handling majorana fermions can be found in Ref. 7 appendices and Ref. 8.

Since our results differ in the sign of interference terms and include new terms we present our matrix element before summing and squaring in appendix A. The complete summed and squared matrix element including non-degenerate left and right chiral squark masses is also included in appendix A. The effect of left-right chiral splitting has been considered previously[1,18] and is expected to be small. In order to simplify the formulas we will not consider this effect and set $M_{\tilde{q}L} = M_{\tilde{q}R} = M_{\tilde{q}}$. In this case we we have for the annihilation channel

$$
\begin{aligned}
|\mathcal{M}|^2 =& 16g^4\Bigg\{(u'^2+v'^2)\left[\frac{(k_1p_1)^2}{(M_{\tilde{q}}^2-t)^2}+\frac{(k_1p_2)^2}{(M_{\tilde{q}}^2-u)^2}-\frac{m_X^2(k_1k_2)}{(M_{\tilde{q}}^2-t)(M_{\tilde{q}}^2-u)}\right]\\
&+2w'^2\left[\frac{(k_1p_1)^2+m_q^2m_X^2}{(M_{\tilde{q}}-t)^2}-\frac{(p_1k_1)^2+(p_1k_2)^2-(k_1k_2)(p_1p_2)+m_q^2m_X^2}{(M_{\tilde{q}}^2-t)(M_{\tilde{q}}^2-u)}\right.\\
&\left.+\frac{(k_1p_2)^2+{m_q}^2m_X^2}{(M_{\tilde{q}}^2-u)^2}\right]+2u'v'\left[\frac{m_q^2m_X^2}{(M_{\tilde{q}}^2-t)^2}+\frac{m_q^2m_X^2}{(M_{\tilde{q}}^2-u)^2}-\frac{m_q^2(p_1p_2)}{(M_{\tilde{q}}^2-t)(M_{\tilde{q}}^2-u)}\right]\\
&+4w'(u'+v')m_qm_X\left[\frac{(k_1p_1)}{(M_{\tilde{q}}^2-t)^2}+\frac{(k_1p_2)}{(M_{\tilde{q}}^2-u)^2}-\frac{(k_1p_1)+(k_1p_2)}{2(M_{\tilde{q}}^2-t)(M_{\tilde{q}}^2-u)}\right]\\
&+\frac{(Z_{13}^2-Z_{14}^2)^2}{\cos^4\theta_w(m_Z^2-s)^2}\left[\frac{1}{4}(c_L^2+c_R^2)\left((k_1p_1)^2+(k_1p_2)^2-m_X^2(k_1k_2)\right)\right.\\
&\left.+\frac{1}{2}c_Lc_Rm_q^2\left((p_1p_2)-2m_X^2\right)\right]
\end{aligned}
$$

$$
\begin{aligned}
&+\frac{(Z_{13}^2-Z_{14}^2)}{2\cos^2\theta_w(m_Z^2-s)}\left[\left(\frac{(k_1p_1)^2}{(M_{\tilde{q}}^2-t)}+\frac{(k_1p_2)^2}{(M_{\tilde{q}}^2-u)}\right)(2v'c_R-2u'c_L)\right.\\
&+\left(\frac{1}{(M_{\tilde{q}}^2-t)}+\frac{1}{(M_{\tilde{q}}^2-u)}\right)\Big[(u'c_L-v'c_R)m_X^2(k_1k_2) \qquad (3)\\
&\qquad +m_q^2(u'c_R-v'c_L)\big(2m_X^2-(p_1p_2)\big)\Big]\\
&\left.+2m_qm_Xw'(c_R-c_L)\Big[\frac{2(k_1p_2)-(k_1p_1)}{(M_{\tilde{q}}^2-u)}+\frac{2(k_1p_1)-(k_1p_2)}{(M_{\tilde{q}}^2-t)}\Big]\right]\Bigg\},
\end{aligned}
$$

where m_X is the neutralino mass, p_1 and p_2 are the incoming $\widetilde{\chi}$ four-momenta, k_1 and k_2 are the outgoing fermion momenta, and (p_1p_2) denotes a four-momentum dot product. The symbols s, t, and u are the usual Mandelstam invariants, $u'=a^2+b^2$, $v'=a^2+c^2$, and $w'=\epsilon a(b-c)$.

The matrix element for the elastic scattering process $\widetilde{\chi}q\to\widetilde{\chi}q$ with momenta labeled $p_1+k_1\to p_2+k_2$ respectively can be found from eq. (3) by crossing $k_2\to -k_1$, $k_1\to k_2$, and $p_2\to -p_2$, so $t\to u$, $u\to s$, and $s\to t$. Likewise, the matrix element for the production process $e^+e^-\to\bar{\widetilde{\chi}}\widetilde{\chi}$ (momenta labeled $p_1+p_2\to k_1+k_2$) is found by $k_1\leftrightarrow p_2$ and $k_2\leftrightarrow p_1$. With these substitutions the labels m_q and m_X remain unchanged.

To find the annihilation cross section we must integrate eq. (3) over the center-of-mass scattering angle. This is tedious due to the angular dependence in the propagator momenta, but we do not actually need this result because we are only interested in using the annihilation cross section to calculate relic abundances. For this purpose one needs a thermally averaged cross section, which is most easily obtained by expanding the relativistic cross section in powers of the relative velocity v. We do this before integrating and keep terms up to order v^2. This method is also satisfactory for calculating neutralino annihilation in the Sun or galactic halo since again the collisions are non-relativistic. We find the annihilation cross section to be

$$\sigma_{ann}v = \sum_q \frac{4}{\pi} G_F^2 c_q m_X^2 \beta' \Bigg\{ y'^4 \Bigg[(u'^2 + v'^2)\big(z^2 + (a_1 + r_1)v^2\big) + 4w'^2\big(1 + (a_2 + r_2)v^2\big)$$
$$+ 4w'(u' + v')z\big(1 + (\frac{1}{4}x^2 + r_3)v^2\big) + 2u'v'z^2\big(1 + (a_4 + r_4)v^2\big)\Bigg]$$
$$+ (Z_{13}^2 - Z_{14}^2)^2 x'^4 \Bigg[\frac{1}{4}(c_L^2 + c_R^2)(z^2 + a_1 v^2) + \frac{1}{2}c_L c_R z^2(-1 - a_4 v^2)\Bigg]$$
$$+ (Z_{13}^2 - Z_{14}^2)x'^2 y'^2 \Bigg[(v'c_R - u'c_L)\big(z^2 + (a_1 + z^2 r_5)v^2\big)$$
$$+ (u'c_R - v'c_L)z^2\big(1 + (a_4 + r_5)v^2\big) - 2w'(c_L - c_R)z\big(1 + (\frac{1}{4}x^2 + r_5)v^2\big)$$
$$v^2\beta'^2 r\Big(-\frac{2}{3}(u'c_L + v'c_R) + w'(c_L - c_R)z\Big)\Bigg]\Bigg\}, \tag{4}$$

where

$$a_1 = \frac{2}{3} - \frac{5}{12}z^2 + \frac{1}{4}z^2x^2$$
$$a_2 = \frac{1}{4}(2 - z^2 + x^2)$$
$$a_4 = \frac{1}{4}(-3 + x^2)$$
$$r_1 = \frac{r}{3}(-4 + z^2 + 4r - 3rz^2 - rz^4)$$
$$r_2 = \frac{r}{3}(-5 + 2z^2 + 3r\beta'^2 + 2rz^2\beta'^2)$$
$$r_3 = \frac{r}{3}(-3 + 5r\beta'^2 - 2\beta'^2)$$
$$r_4 = \frac{r}{3}(-3 + 5r\beta'^2)$$
$$r_5 = \frac{r}{3}(-\frac{3}{2} + r\beta'^2),$$

where G_F is the Fermi constant, c_q is a color factor, 3 for quarks, 1 for leptons, $x'^2 = m_Z^2/((m_Z^2 - s)^2 + \Gamma_Z^2 m_Z^2)^{1/2}$ is the Z^0 pole factor, Γ_Z is the Z^0 width, $z = m_q/m_X$, $\beta' = (1 - z^2)^{1/2}$, and $y'^2 = m_W^2/(M_{\tilde{q}}^2 + \beta'^2 m_X^2)$ is the squark mass suppression including the propagator momentum. The propagator momenta factor $r = m_X^2/(M_{\tilde{q}}^2 + \beta'^2)$ is usually small, as is $x^2 = \frac{1}{2}z^2/(1 - z^2)$. When $m_X \to m_q$

however, $z \to 1$, $x \to \infty$, and the expansion breaks down. This occurs only very near mass thresholds, so we avoid evaluating eq. (4) right at threshold. The effect of ignoring propagator momenta can be found by taking the limits $y' \to m_W/M_{\tilde{q}}$ and $r \to 0$ in eq. (4).

As a check, we can consider the pure photino (or pure higgsino) limit of eq. (4). A pure photino has $Z_{13} = Z_{14} = a = 0$, $Z_{11} = \cos\theta_w$, $Z_{12} = \sin\theta_w$ and $b = c = e_q \sin\theta_w$. The annihilation cross section becomes

$$\sigma_{ann} v(\text{photino}) = \sum_q \frac{8\pi\alpha^2 c_q e_q^4 m_X^2 \beta'}{(M_{\tilde{q}}^2 + m_X^2 \beta'^2)^2} \left\{ z^2 + \frac{1}{3}v^2 \left[1 - \frac{7}{4}z^2 + \frac{3}{4}z^2x^2 - 2r + 2r^2 - rz^2 + r^2z^2 - 3r^2z^4 \right] \right\}. \tag{5}$$

In the no propagator momenta limit we recover the well-known[5,12,19] formula for the photino. We can also recover a higgsino by taking $b = c = Z_{11} = Z_{12} = 0$, and $Z_{13} = \sin\beta$, $Z_{14} = \cos\beta$. We perform the thermal average in the standard manner by replacing v^2 with $6T/m_X$ where T is the temperature, although this is not strictly correct to this order in v^2.[20]

The above neutralino cross section, eq. (4), differs from previous work[9] in several ways. First it includes the effect of propagator momenta which can be important if the neutralino is near in mass to the squark or slepton. Even for the pure photino, this effect can be important as is discussed in Sec. V and shown in Fig. 10. Second, several new terms appear which can be important or not depending on parameters. Third, we find opposite signs for the b^2 and c^2 terms, an important effect when Z^0 – squark interference occurs.

To find the elastic scattering cross section we cross the matrix element as described above and integrate over the center-of-mass scattering angle. Since we are interested in the scattering of neutralinos from the halo of our galaxy, and the velocity of halo particles is known to be $v_{halo} \sim 10^{-3}$, we can take an extreme non-relativistic limit. This greatly simplifies the formulas. In particular, $s \to (m_X + m_q)^2$, $t \to 2|\vec{p}_1|^2(1 - \cos\theta^*)$, $u \to (m_X - m_q)^2$, and so if we can ignore the small mass of the quark, we have $s \approx u$ and $t \approx 0$. Taking the limit

$M_{\tilde{q}L} = M_{\tilde{q}R} = M_{\tilde{q}}$ we find

$$\sigma_{el} = \frac{8G_F^2 m_X^2 {m_q}^2}{\pi(m_X + m_q)^2}\left\{3\left[(2a^2+b^2+c^2)\bar{x}_q^2 + \frac{1}{2}(c_R - c_L)(Z_{13}^2 - Z_{14}^2)\right]^2 + 4\bar{x}_q^4 a^2(b-c)^2\right\}, \tag{6}$$

where $\bar{x}_q^2 = m_W^2/(M_{\tilde{q}}^2 - m_X^2)$. We are actually more interested in scattering off nuclei than off quarks, and this will be discussed in the next section. Taking the pure photino limit we find

$$\sigma_{el}(\text{photino}) = \frac{48\pi\alpha^2 e_q^4 m_X^2 {m_q}^2}{(m_q + m_X)^2(M_{\tilde{q}}^2 - m_X^2)^2}, \tag{7}$$

which, apart from the newly included propagator correction to the scalar fermion mass, reproduces the well known formula.[5,12] A pure higgsino result can also be easily found.

Finally, we wish to be able to include constraints on the parameter space from the ASP experiment.[15] This experiment measured the cross section for e^+e^- going to photon plus missing energy at the PEP storage ring at SLAC ($\sqrt{s} = 29$ GeV). With their luminosity, the Standard Model background from $e^+e^- \to \bar{\nu}\nu\gamma$ is predicted to be .03 pb, and from their limit of $\sigma(e^+e^- \to \gamma + \text{missing}) \leq .06$ pb, we get a limit on the production of neutralinos of $\sigma(e^+e^- \to \bar{\tilde{\chi}}\tilde{\chi}\gamma) \leq .03$ pb.[24] In the soft photon limit valid here, the desired cross section can be calculated from $\sigma(e^+e^- \to \bar{\tilde{\chi}}\tilde{\chi})$ using the formula[26]

$$\frac{d\sigma(e^+e^- \to \gamma X\bar{X}; s)}{dxdy} \simeq \frac{2\alpha}{\pi}\frac{\left[(1-\frac{1}{2}x)^2 + \frac{1}{4}x^2y^2\right]}{x(1-y^2)}\sigma(e^+e^- \to X\bar{X}; \hat{s}) \tag{8}$$

where s is the Mandelstam variable, $x = 2E_\gamma/\sqrt{s}$ is the dimensionless photon energy, $y = \cos\theta$ is the angle between the beam and the photon, and $\hat{s} = s(1-x)$. Performing the crossing described above, setting the electron mass to zero and

taking the limit $M_{\tilde{q}L} = M_{\tilde{q}R} = M_{\tilde{q}}$ we find

$$\sigma(e^+e^- \to \bar{q}q) = \frac{2}{3\pi} G_F^2 s \left(1 - \frac{4m_X^2}{s}\right)^{\frac{3}{2}} \Big[x_q^4 (b^4 + c^4) + x_q^2 x'^2 (Z_{13}^2 - Z_{14}^2)(c_R c^2 - c_L b^2) + \frac{1}{4} x'^4 (Z_{13}^2 - Z_{14}^2)^2 (c_L^2 + c_R^2) \Big], \tag{9}$$

where $x_q = m_W / M_{\tilde{q}}$ and we have not included the propagator momenta here. The pure photino limit of eq. (9) agrees with previous work.[21] (See also Ref. 22).

III. Effective Lagrangian and elastic scattering off nuclei

The cross sections presented in Sec. II are for neutralino interactions with quarks or leptons, while for direct detection, or capture into the body of the Earth or Sun, the interaction between neutralinos and nuclei is needed. For this purpose, it is useful to re-derive some of the above using an effective Lagrangian approach. Since previous calculations[9] have used this approach it is also useful for comparison purposes.

We start from the supersymmetric Lagrangian interaction terms given in Refs. 7 and 8, and consider only the limit of heavy scalar fermions. We have

$$\begin{aligned} L_{eff} = & \frac{-4g^2}{M_{\tilde{q}L}^2} \bar{\tilde{\chi}}(aP_R + bP_L) q \bar{q} (aP_L + bP_R) \tilde{\chi} \\ & - \frac{4g^2}{M_{\tilde{q}R}^2} \bar{\tilde{\chi}}(cP_R - aP_L) q \bar{q} (cP_L - aP_R) \tilde{\chi} \\ & - \frac{g^2}{2m_W^2} (Z_{13}^2 - Z_{14}^2) \bar{q} \gamma^\mu (c_L P_L + c_R P_R) q \bar{\tilde{\chi}} \gamma_\mu \gamma_5 \tilde{\chi}, \end{aligned} \tag{10}$$

where q is the quark field, and the other symbols were defined in Sec. II.. To get eq. (10) in a more useful form we perform Fierz transformations on the first two

terms. Using the fact[7] that for Majorana fermions $\bar{\tilde{\chi}}\gamma_\mu\tilde{\chi} = 0$ we find

$$L_{eff} = \frac{g^2}{2m_W^2}\left\{\bar{\tilde{\chi}}\gamma_\mu\gamma_5\tilde{\chi}\bar{q}\gamma^\mu(V' + A'\gamma_5)q + 2a\epsilon(bx_{qL}^2 - cx_{qR}^2)[\bar{\tilde{\chi}}\tilde{\chi}\bar{q}q + \bar{\tilde{\chi}}\gamma_5\tilde{\chi}\bar{q}\gamma_5 q]\right\}, \tag{11}$$

where

$$\begin{aligned} V' &= -\frac{1}{2}(c_R + c_L)(Z_{13}^2 - Z_{14}^2) + x_{qL}^2(b^2 - a^2) + x_{qR}^2(a^2 - c^2) \\ A' &= \frac{1}{2}(c_L - c_R)(Z_{13}^2 - Z_{14}^2) - x_{qL}^2(a^2 + b^2) - x_{qR}^2(a^2 + c^2), \end{aligned} \tag{12}$$

and where $x_{qL} = m_W/M_{\tilde{q}L}$, etc.. Later we will include the effect of propagator momenta by substituting $\bar{x}_{qL}$ for x_{qL} etc.. For the limiting case of pure photino or pure higgsino eq. (11) agrees with the corresponding limiting cases of Ellis *et al.*. For the general neutralino, however, there are several differences. First, there is a new term which is not of the form of an axial vector coupling. In the limit of equal left and right chiral squark masses, it is proportional to $(b - c)$, the zino coupling, and to a, the higgsino coupling. This term may have been ignored previously because higgsinos, like Higgs bosons, couple proportional to mass, and for quarks or leptons this is usually quite small. However, for low energy elastic scattering off nuclei, Higgs bosons,[11] as well as higgsinos couple proportional to the nuclei mass, not the quark mass, and so this new scalar term can be important. Second, the sign of the b^2 and c^2 terms (or equivalently the $(Z_{13}^2 - Z_{14}^2)$ and a^2 terms, since the overall sign is arbitrary) differ from Ellis *et al.*. Since in annihilation, for example, the a^2 term is usually small, the primary effect of this sign difference is negative Z^0-squark interference, where before there was positive interference (and vice-versa). We shall show that this interference results in low direct detection rates for parts of parameter space.

The effective Lagrangian, eq. (11) can be used to calculate the annihilation, elastic, and production cross sections in the standard manner. For the annihilation cross section there are several terms which appear in the complete cross section, eq.(4), which do not appear in the cross section calculated from the effective Lagrangian. For the elastic cross section in the extreme non-relativistic limit

we find that the pseudo-scalar term does not contribute, and from the complete calculation, eq. (6), we also see that there is no interference between the axial vector and scalar terms. In fact, eq. (11) reproduces eq.(6) except for propagator momenta.

We now use eq. (11) to find scattering off of nuclei. This is done by first finding $\sum_q |\langle N|L_{eff}|N\rangle|^2$, where $|N\rangle$ is the nucleus wave function, which is assumed to be a sum of nucleon wave functions $|n\rangle$, which are in turn assumed to be sums of quark wave functions. The axial vector piece of the elastic cross section can be evaluated as in Goodman and Witten[1] and we find the elastic scattering cross section off a nucleus of mass m_N to be

$$\sigma_{el} = \frac{24 m_X^2 m_N^2 G_F^2}{\pi (m_X + m_N)^2} \left\{ \frac{4}{3}\lambda^2 J(J+1) \left(\sum_{u,d,s} A' \Delta q \right)^2 + \left(\frac{2m_N}{27 m_W} \right)^2 \left(\sum_{c,b,t} (b-c) x_q^2 d_q \right)^2 \right\}, \tag{13}$$

where J is the total spin of the nucleus and the sums are over the indicated quarks. The first term agrees with Ref. 1 in the photino limit (see also Ref. 19) and the second term is new and requires some explanation. In the above, we followed Goodman and Witten,[1] and Refs. 23 and 18 in defining

$$\lambda = \frac{1}{2}\{1 + [s_p(s_p+1) - l(l+1)]/[J(J+1)]\} \tag{14}$$

from the one particle nuclear shell model[27] and the Lande formula, where l is the shell model angular momentum and s_p is the proton (or neutron) spin. We also follow Refs. 16, 23 and 18 in defining $\langle p|\bar{q}\gamma_\mu\gamma_5 q|p\rangle = 2\Delta q \vec{s}_q$, where $\vec{s}_q$ is the spin of quark q and Δq measures the fraction of the proton spin carried by quark q. Under some assumptions, the EMC group[16] gives $\Delta u = .746$, $\Delta d = -.508$ and $\Delta s = -.226$, while the flavor SU(3) quark model predicts $\Delta u = .97$, $\Delta d = -.28$ and $\Delta s = 0$. The EMC results are still controversial, so for most of our work

we use the flavor SU(3) values. In Sec. VII we show the effect of using the EMC values. Note that for simplicity we left out vector pieces in Eq. (11) which can be important if there is significant left and right chiral squark mixing. These terms have been discussed in Refs. 1 and 18 and are expected to be small.

In deriving the second term of Eq. (13) we modified slightly a technique described in Shifman *et al.*[11] and used recently by Raby and West.[28] For coherent scattering of a neutralino off a nucleus we need to find

$$\langle N|\sum_q 2a(b-c)x_q^2\bar{q}q|N\rangle \propto \langle N|\sum_q T_{3L}x_q^2 d_q m_q\bar{q}q|N\rangle, \tag{15}$$

where $\langle N|$ is the nucleus state and the sum is over all the quarks, both valence and sea. Using the "heavy quark expansion" for the charm, bottom and top quarks Shifman *et al.* write $m_q\bar{q}q \simeq -\frac{2}{3}\frac{\alpha_s}{8\pi}G^a_{\mu\nu}G^a_{\mu\nu} + O\left(\frac{\alpha_s^2}{m_q^2}\right)$ and by including the anomaly in the trace of the quark energy-momentum tensor $\theta_{\mu\mu}$ they find

$$m_N\bar{\Psi}_N\Psi_N = \langle N|\theta_{\mu\mu}|N\rangle \simeq -\frac{9\alpha_s}{8\pi}\left\langle N|G^a_{\mu\nu}G^a_{\mu\nu}|N\right\rangle. \tag{16}$$

Physically, this last equation says that the mass of the nucleon (and therefore the nucleus) comes from the light quark anomaly. Since the light quarks in eq. (15) are very light, we can follow Shifman *et al.* in ignoring them and find

$$\langle N|\sum_q 4aT_{3L}x_q^2\bar{q}q|N\rangle \simeq \left(\frac{4m_N}{27m_W}\right)\sum_{c,b,t}T_{3L}x_q^2 d_q \simeq \frac{2m_N x_q^2}{27m_W}\left(\frac{2Z_{14}}{\sin\beta} - \frac{Z_{13}}{\cos\beta}\right), \tag{17}$$

where in the last step we made the simplifying assumption that all squarks have the same mass. Using Eq. (17), one finds Eq. (13) in a straightforward manner.

The essence of the above derivation is that neutralinos can couple to the gluons in the nucleon via a loop involving heavy quarks and a squark. In the limit of very heavy squarks this becomes the same loop as Shifman *et al.* discuss for the Higgs exchange case. Since the higgsino, like the Higgs boson, couples proportional to the mass of the quark in the loop, the quark mass cancels out

and one is left with a coupling to the gluons which does not involve (to lowest order) the heavy quark mass. As mentioned above, the light quark glue gives rise to the mass of the nucleon, and so the final coupling is proportional not to the quark mass, but to the nucleon mass. For dark matter neutralinos from the galactic halo we can sum coherently over all the nucleons in the nuclei and arrive at a coupling proportional to the mass of the nucleus. Actually, when a heavy neutralino scatters off of a heavy nucleus some loss of coherence is possible and we take this effect into account in Sec. V. We do not claim that the above cross section, eq. (13) is exact, but it shows that "spin independent" cross sections exist for Majorana particles. Uncertainties include the extent to which the charm, bottom and top quarks contribute equally, the extent to which the strange quark contributes, the possibility of additional generations of quarks, and higher order contributions, both in the heavy quark and the heavy squark expansions.

Finally note that we have included the effect of propagator momenta for the elastic cross section, eq. (13), by using $\bar{x}_q$, instead of x_q in A' as derived in the complete elastic cross section. This can have a substantial effect if m_X is near $M_{\tilde{q}}$, as illustrated in Sec.V.

IV. Relic Abundance and LSP constraints

Using eq. (4) the present day mass density of neutralinos can be calculated. This "Lee-Weinberg" calculation[29] has been the subject of many papers and we will use the method described in Refs. 30 and 31, which is an extension of the methods described in Ref. 32. This is an approximate analytic solution to the Boltzman equation $\dot{n} = -3Hn - \langle\sigma v\rangle_{ann}(n^2 - n_0^2)$, which governs the number density n of particles as the universe cools. Here H is the Hubble parameter, n_0 is the equilibrium number density of neutralinos and $\langle\sigma v\rangle_{ann}$ is the thermally averaged annihilation cross section derived in Sec. II. The basic idea is that when the temperature T of the radiation in the universe falls below the mass of the neutralino, the neutralino number density is suppressed by a Boltzman factor $e^{-E/T}$ and falls rapidly. But since the interaction of neutralinos with ordinary matter is weak, there comes a time (denoted as freeze-out) after which

annihilation of neutralinos becomes improbable and the neutralinos present then are, for the most part, still present today. Our approximation uses an accurate method of finding the freeze out temperature, includes properly the effect of changing degrees of freedom and is accurate to better than 5% (as compared to a numerical integration). The reader is referred to Refs. 30 and 31 for more details.

Figs. 2a,b,c show "scatter plots" of $\Omega_{\tilde{\chi}}h^2$ versus the mass, m_X, of the neutralino, where $h = H/(100 \text{ km sec}^{-1} \text{ Mpc}^{-1})$. These figures were made by selecting a value of $M_{\tilde{q}}$ and $\tan\beta$ and considering a grid of points in the M, μ plane. For each set of the four parameters M, μ, $\tan\beta$, and $M_{\tilde{q}}$ we find m_X and $\langle\sigma v\rangle_{ann}$, and then the relic abundance $\Omega_{\tilde{\chi}}h^2$. Each "x" in the figure represents a different supersymmetric model,and the collection of x's indicate the range of relic abundances possible. There are several interesting features in these figures.

First, notice that over a very wide range of supersymmetric parameters almost no models give $\Omega_{\tilde{\chi}}h^2 < .01$., (The lines across the figures indicate $\Omega_{\tilde{\chi}} = 1$ for our preferred value $h = \frac{1}{2}$) the primary exception being at $m_X \sim m_Z/2$, where annihilation is greatly enhanced due to the Z^0 pole. The values of $M_{\tilde{q}}$ and $\tan\beta$ in Figs. 2a, 2c were selected because they give low values for $\Omega_{\tilde{\chi}}h^2$; values of $M_{\tilde{q}}$ of less than 50 GeV being inconsistent with results from the UA1 experiment at CERN.[13] The "wedge"'s on the left of the figures consist of models where the neutralino contains substantial higgsino content and move upward in $\Omega_{\tilde{\chi}}h^2$ as $\tan\beta$ moves away from 1. The "lines"'s through the Z^0 pole consist of models with a photino-like neutralino and also move upward in $\Omega_{\tilde{\chi}}h^2$, this time as the (assumed degenerate) scalar fermion masses increase. Recalling that the total luminous matter in the universe contributes $\Omega \simeq .01$, the observed dynamical (dark) mass contributes $\Omega \simeq .1 - .3$, and nucleosynthesis limits baryonic matter to $.015 \leq \Omega h^2 \leq .16$, we see that if low energy supersymmetry exists and the neutralino is the LSP, it almost certainly is a significant component of the universe. This is true whether or not it is the main component of dark matter in galactic halos. Since m_X is in the GeV range, neutralinos constitute cold dark matter and should cluster in galactic halos, so we consider it likely that galaxies contain as much or more mass in the form of neutralinos as in the form of baryons. This likelihood alone is enough to justify experimental attempts to detect neutralino

DM. It is also seen from Fig. 2 that a wide range of parameters predict a critical density of neutralinos ($\Omega_{\tilde{\chi}}h^2 = 1/4$) and that much of parameter space is ruled out by requiring $\Omega_{\tilde{\chi}} \leq 1$. Since $\Omega_{\tilde{\chi}} = 1$ arises naturally and since $\Omega = 1$ is desirable for several theoretical reasons, in this Report we will use the constraint $\Omega_{\tilde{\chi}}h^2 = 1/4$ to reduce the parameter space which must be explored. As mentioned in the introduction, galactic neutralinos may be detectable and many of the items discussed in this Report may be relevant even if $\Omega_{\tilde{\chi}} < 1$, especially since Fig. 2 suggests that $\Omega_{\tilde{\chi}}$ is likely to be greater than 4%. In fact, lowering $\Omega_{\tilde{\chi}}$ requires an increase in coupling strengths causing neutralinos to interact more strongly in a detector.

To begin to develop intuition about the neutralino parameter space we show in Figs. 3a,b,c,d contours of $\Omega_{\tilde{\chi}}h^2 = 1/4$ in the M, μ plane for several values of $\tan\beta$ and $M_{\tilde{q}}$. For typical values of $\tan\beta$ and $M_{\tilde{q}}$ there is a "closed curve" in the middle of the figure and a "hyperbola" in the upper right hand corner. The contours are sometimes broken; small gaps resulting from the finite grid size in our contour finding program, and large gaps showing areas where no solution exists. No solution may exist when a neutralino mass eigenvalue crossing occurs and the resulting discontinuity in neutralino composition causes a discontinuity in relic abundance. For brevity, we will call a piece of broken contour a "strand" (as in spaghetti). These strands will be the building blocks of most of the figures in the remainder of this Report. We map the strands onto various other parameter spaces and use consistency and accelerator experiment results, which constrain the parameter space, to chop pieces off the strands. This is not, perhaps, the ideal way to present our results, but four (at least) dimensional parameter space is difficult to display. Note that Figs. 3a,b show the $\mu > 0$ case while Figs. 3c,d show the $\mu < 0$ case.

As an important first example, consider the consistency constraint that the neutralino be the LSP. In a given model $M_{\tilde{q}}$ is specified and so any values of M, μ, and $\tan\beta$ which result in $m_X > M_{\tilde{q}}$ are ruled out. For example, all the models in Fig. 2a (with $M_{\tilde{q}} = 50$ GeV) to the right of $m_X = 50$ GeV are inconsistent with the neutralino being the LSP and should not be considered. Throughout we discard regions of parameter space which do not satisfy $m_X < M_{\tilde{q}}$.

Another important consistency constraint comes from the charginos, the supersymmetric partners of the charged Higgs bosons. The neutralino parameters M, μ, and $\tan\beta$ determine uniquely the masses $m_{\tilde{\chi}^\pm}$ and couplings of the two charginos. Accelerator experiments constrain these masses and this will be discussed in Sec. VI, but here we only consider the consistency constraint $m_X < m_{\tilde{\chi}^\pm}$. Figs. 4a,b show contours of $m_X = m_{\tilde{\chi}^\pm}$ for several values of $\tan\beta$ and $\mu > 0$. The areas between the two contours correspond to $m_{\tilde{\chi}^\pm} < m_X$ and are therefore inconsistent. Fig. 4a shows the $m_X = m_{\tilde{\chi}^\pm}$ contours on top of the $\Omega_{\tilde{\chi}} h^2 = 1/4$ contour for one value of $M_{\tilde{q}}$ and $\tan\beta$. Note that much of one stand lies between the $m_X = m_{\tilde{\chi}^\pm}$ contours. This is a generic feature when $\mu > 0$ and cuts out considerable parameter space. (For $\mu < 0$, we find $m_X < m_{\tilde{\chi}^\pm}$ almost everywhere and this constraint has little effect.) This loss of parameter space will show up later as breaks or gaps in the projected strands. Fig. 4b shows the $m_X = m_{\tilde{\chi}^\pm}$ contours for several values of $\tan\beta$.

V. Direct detection

In this section we apply the elastic scattering cross section, eq. (13), to scattering from various elements and give the rates for neutralino interaction in a cryogenic detector. This new class of detectors plans to measure the small (order keV) energy deposited when a particle from the galactic halo hits a nucleus in the detector. Ionization detectors now operating with energy thresholds of order 5 keV have already ruled out Dirac neutrinos with masses greater than 20 GeV as the major component of the galactic halo.[33] Many groups are developing new non-ionization cryogenic detectors which will operate at lower temperatures to reduce the background and lower the energy threshold.

The rate of detection in a cryogenic detector is given in Ref. 3 (and verified by us) as

$$R = \sqrt{\frac{8}{3\pi}}\eta_t\eta_v\eta_c \frac{\langle v\rangle_{halo}\,\rho_{halo}\sigma_{el}}{m_N m_X}, \tag{18}$$

where σ_{el} is the elastic cross section, eq. (13), $\langle v\rangle \simeq 270$ km/sec is the average dispersion velocity in the halo, η_v is a correction due to the motion of the Sun and

the Earth and η_t corrects for the energy threshold. Including only the motion of the Sun for simplicity, we find $\eta_v \simeq 1.3$. The factor η_c estimates the loss of coherence which occurs at high momentum transfer when neutralinos start to interact with individual nucleons rather than the nucleus as a whole. Using the form factor from Ref. 3

$$\eta_c = \alpha^{-2}\left(\frac{1}{2} + p'^2 + \frac{p' e^{-p'^2}}{\sqrt{\pi}\mathrm{erf}p'}\right)^{-1}\left[1 - \left(\frac{\exp\left(\frac{-p'^2\alpha^2}{1+\alpha^2}\right)\mathrm{erf}\left(\frac{p'}{\sqrt{1+\alpha^2}}\right)}{\sqrt{1+\alpha^2}\mathrm{erf}p'}\right)\right], \quad (19)$$

where

$$\alpha^2 \simeq \frac{.83(m_X/40\ \mathrm{GeV})^2}{(m_X/m_N+1)^2}\left[(m_N/200\ \mathrm{GeV})^{1/3} + .06\right]^2 (\langle v\rangle/270\ \mathrm{km\ sec}^{-1}), \quad (20)$$

and $p' = \sqrt{\frac{3}{2}} v_{sun}/\langle v\rangle \simeq 1$. For convenience we give a plot of η_c as a function of m_N and m_X in Fig. 5. It is a substantial correction for heavy DM particles ($m_X > 50$ GeV) and for heavy nuclei ($m_N > 100$ GeV). Note that for simplicity, we have taken a zero energy threshold throughout ($\eta_t = 1$). The actual value of η_t depends upon detector design and is most important for light nuclei and light DM particles.

In Fig. 6 we show the event rates in a mercury detector (natural abundance) plotted against the neutralino mass for several supersymmetric models. Fig. 6a is the total rate, while Fig. 6b shows the axial vector rate (without the new scalar term) and Fig. 6c shows the scalar interaction rate alone. Figs. 6a, b, c show the $\mu > 0$ case, while Figs. 6d, e, f show the $\mu < 0$ case. We chose mercury not because it is an especially promising element, but because it emphasizes the possible importance of the new scalar term. It is heavy, and since $\lambda^2 J(J+1) = 1/12$ for the 17% of Hg which has a spin, it has very low rates for the pure axial vector coupling. Figure 7 is the same as Fig. 6 but for fluorine (7a,b), a light element which is 100% a spin $\frac{1}{2}$ isotope with favorable shell parameters ($\lambda^2 J(J+1) = 3/4$) and for thallium (7c), a heavy element with 100% $\lambda^2 J(J+1) = 3/4$. For fluorine the axial vector term dominates almost everywhere while for thallium the scalar

and axial vector contributions are comparable. The lines in the figure correspond to "strands" in the M, μ plane for which $\Omega_{\tilde{\chi}} h^2 = 1/4$ as discussed in Sec. IV. Various values of $M_{\tilde{q}}$ and $\tan\beta$ are shown. All squark and slepton masses have been taken degenerate; the non-degenerate case will be discussed in Sec. VII.

The rates shown here are easily scaled to other elements with the same one-particle-shell-model structure (Hg is a shell model "neutron", while F and Tl are "proton"'s). The axial vector rate is scaled by

$$\frac{[\lambda J(J+1)]_N}{[\lambda J(J+1)]_{\rm Hg}} \frac{m_N}{m_{\rm Hg}} \frac{(m_{\rm Hg}+m_X)^2}{(m_N+m_X)^2} \frac{f_N}{f_{\rm Hg}}, \tag{21}$$

where f_N is the relative abundance of the relevant isotope, while the scalar term is scaled by

$$\frac{m_N^3}{m_{\rm Hg}^3} \frac{(m_{\rm Hg}+m_X)^2}{(m_N+m_X)^2} \frac{(\eta_c)_N}{(\eta_c)_{\rm Hg}}. \tag{22}$$

For germanium, which is modeled as a "neutron" for example, these factors are roughly 4 and .4 respectively for light neutralinos. For elements which are not describable by single-particle protons or neutrons the sum over $A'\Delta q$ must be redone to get the axial vector rate. The scalar rate is still given by the formula above.

Figures 6 and 7 show several important features. First note the wide range in rates possible at a given m_X which comes from considering the general neutralino rather than just the pure photino. (See Ref. 18 for another recent discussion of this point.) A large percentage of the bottoms of the strands in the loops in Fig. 3 represent almost pure photino states and these strands cluster in the large "pure photino" blobs seen at around 3 and 30 GeV. The rate for a pure photino depends only on $M_{\tilde{q}}$ so there is one blob for $M_{\tilde{q}} = 50$ GeV and one for $M_{\tilde{q}} = 125$ GeV. The variation in rate is perhaps over-emphasized with Hg where, as a shell model neutron, the axial vector rate is extremely small, due in part, to the quark model flavor SU(3) spin structure functions. (See Ref. 36 for the rates for Hg with EMC structure functions.) Thallium is also heavy, but is a shell model proton and has favorable shell model parameters and shows much less spread in the total

rate. However, the axial vector rate alone drops below 10^{-4} events/kg/day in several places due to the cancellations described below.

Next note the large dip in rate at $m_X \simeq m_Z/2 \simeq 45$ GeV. The Z^0 pole makes annihilation of 45 GeV neutralinos very efficient, so small values of the couplings are needed for $\Omega_{\tilde{\chi}} = 1$. These small couplings remain in the elastic cross section, where the Z^0 pole is not present, resulting in low rates. A neutralino with $m_X \simeq m_Z/2$ would be difficult to detect directly, though its suppression here implies an enhancement in Z^0 decay or accelerator production. In Figure 6b (axial vector term) there are also large dips in event rate at $m_X \simeq 6$ GeV and $m_X \simeq 20$ GeV. These are another generic feature and come about from negative Z^0-squark interference. (There is, in addition, cancellation among the terms in the sum over $A'\Delta q$.) The values $m_X \simeq 6$ and $m_X \simeq 20$ are not special, and as $M_{\tilde{q}}$ and $\tan\beta$ are varied these cancellations occur for all values of m_X. These low rates are mitigated by the contribution from the scalar term as seen in Figs. 6a and 7a. Even for fluorine, where the scalar term is small elsewhere, it dominates here and gives a minimum value for the elastic cross section. Another thing to note is that the pure photino blobs become lines as $M_{\tilde{q}}$ is varied, and that they do not move from Fig. 6a to Fig. 6b showing that the scalar term does not contribute to pure photino elastic scattering.

In order to get a feel for the four dimensional parameter space we show in Fig. 8 the effect of varying $M_{\tilde{q}}$ with $\tan\beta$ fixed, and in Fig. 9 the effect of varying $\tan\beta$ with $M_{\tilde{q}}$ fixed. Keep in mind that reduction of the parameter space will result in further "chopping" of the strands when we include constraints from accelerator experiments in the next section.

Finally, we note that the inclusion of propagator momenta has had a significant effect when m_X neared $M_{\tilde{q}}$. The largest effect was in the annihilation cross section which decreased, thereby requiring an *increased* coupling strength for a given $\Omega_{\tilde{\chi}}$. The increased coupling strength increased the event rate, which was further increased by the inclusion of propagator momenta in the elastic cross section. For the general neutralino, the curves in Figs. 6 and 7 differ when propagator momenta are ignored, but the trend is hard to see. For the pure photino, however, the requirement $\Omega_{\tilde{\chi}} h^2 = 1/4$ fixes the squark mass as a function of m_X,

which in turn fixes the event rate. In Fig. 10 we show the event rate in a fluorine cryogenic detector both with and without propagator momenta included. At $m_X \simeq 10$ GeV, the rate is 30% higher with propagator momenta, at $m_X \simeq 30$ GeV it is double, and by 90 GeV it is more than five times higher. If no new channels or particle thresholds appear, we note that the rate for pure photino detection reaches a minimum at about $m_X = 130$ GeV and then starts to rise again as m_X approaches $M_{\tilde{q}}$.

VI. Accelerator constraints

We have so far used cosmological predilection ($\Omega_{\tilde{\chi}} = 1$) and consistency requirements ($M_{\tilde{q}}, m_{\tilde{\chi}^\pm} > m_X$) to reduce the rather large parameter space in which neutralino dark matter lives. In our selection of values of μ, M, $\tan\beta$, and $M_{\tilde{q}}$ we have also implicitly used theoretical prejudice ($\tan\beta$ not too different from 1, soft supersymmetry breaking parameters less than 1 TeV) and accelerator results[13] ($M_{\tilde{q}} > 50$ GeV). In this section we will further restrict the parameter space by including the result from PETRA[14] that $m_{\tilde{\chi}^\pm} > 23$ GeV and the result from ASP[15] that $\sigma(e^+e^- \to \bar{\tilde{\chi}}\tilde{\chi}\gamma) \leq .03$ pb. The first experiment restricts parameter space because the same three parameters: μ, M, and $\tan\beta$ which determine the neutralino mass and couplings also determine the chargino mass and couplings. (The charginos are the supersymmetric partners of the two charged Higgs bosons.) The ASP experiment is relevant because the $e^+e^- \to \bar{\tilde{\chi}}\tilde{\chi}$ cross section is related to the $\bar{\tilde{\chi}}\tilde{\chi} \to e^+e^-$ cross section. In fact, in general, accelerator experiments are important for particle DM detection since the DM particles may first be found there, and because negative results bear on the feasibility of direct detection. Since limits from experiments will continue to improve it is important to know what parts of parameter space are affected.

Figure 11 shows contours of $m_{\tilde{\chi}^\pm} = 23$ GeV in the μ, M plane for several values of $\tan\beta$. Fig. 11a shows $\mu > 0$ and Fig. 11b shows $\mu < 0$. The areas between the contours in Fig. 11a have $m_{\tilde{\chi}^\pm} < 23$ GeV and are ruled out, while the areas outside the contours are ruled out in Fig. 11b. The effect this has on our spaghetti rate plots (Figs. 6a,d) is shown in Fig. 13, where the ruled out

areas are marked with "x"'s. For $\mu > 0$ many of the models with $m_X < 10$ GeV have been eliminated. Pure photinos, however, are relatively unaffected by this constraint (Note the "blob" at 3 GeV is not "x"'ed out.) since they occur mostly near the $M = 0$ axis, and the affected areas between the contours in Fig. 11a contain mostly models where the neutralino has substantial higgsino and zino components. We note that if the limit on the chargino mass was pushed to $m_{\tilde{\chi}^\pm} > 40$ GeV, most of the parameter space with $m_X < 20$ GeV (except for pure photinos) would be ruled out. Conversely, if a chargino was discovered with $m_{\tilde{\chi}^\pm} < 40$ GeV we would have a good idea of the neutralino mass and couplings. Figure 13a shows the $\mu > 0$ case, while Fig. 13b shows the $\mu < 0$ case. For $\mu < 0$ the chargino constraint is not nearly as important because much less area is ruled out.

The ASP experiment,[15] performed at the PEP storage ring at SLAC, and similar experiments,[26] in principle actually produce neutralinos. These are neutrino counting experiments whose primary aim is to limit the cross section $\sigma(e^+e^- \rightarrow \gamma\bar{\nu}\nu)$, where the photon is detected and the presence of the neutrinos is inferred from their missing energy. For neutralinos with mass below the ASP threshold ($\sim \sqrt{s}/2 \sim 14.5$ GeV), the corresponding process $e^+e^- \rightarrow \bar{\tilde{\chi}}\tilde{\chi}\gamma$ can take place and the ASP limit of $\sigma(e^+e^- \rightarrow \gamma + \text{missing}) \leq .06$ pb (90% confidence level) can be used to rule out those areas of neutralino parameter space which would exceed this. Actually, the neutrino production process must exist as a background ($\sigma(e^+e^- \rightarrow \bar{\nu}\nu\gamma) \sim .03$ pb) and the rate for production of exotic particles is then $\sigma_{\text{exotic}} < .03$ pb. The ASP group[15] has used used this limit to produce restrictions on pure photino parameter space, that is, the selectron mass, and find $M_{\tilde{l}} > 62$ GeV for $m_X = 0$. However, a Bayesian analysis of the same data[25,15] results in the weaker bound $\sigma_{\text{exotic}} < .046$ pb, giving $M_{\tilde{l}} > 58$ GeV for $m_X = 0$. Both statistical methods have problems, and since a recent report[34] combines Bayesian analysis and the results from other experiments to arrive at a number near 68 GeV for the selectron mass, we will use the stronger (and simpler) limit $\sigma_{\text{exotic}} < .03$ pb here.

We have integrated eq. (8) over the ASP acceptance $20 < \theta < 160$ degrees, $E_{max} > 12$ GeV, and $p_T > .8$ GeV/c, and show in Fig. 12 contours of $\sigma(e^+e^- \rightarrow$

$\tilde{\chi}\tilde{\chi}\gamma) = .03$ pb for $\mu > 0$. The areas below the long contours and within the wedges at the right are ruled out at the 90% confidence level. The contours for the $\mu < 0$ case are very similar, the only differences being that the long contours extend straight through to the right edge, and that there are no "wedges"'s. In contrast to the PETRA chargino constraint, we see that for $\mu > 0$ this experiment affects mostly photino neutralinos and has little effect on the rest of parameter space. (See also the recent report of of Tata *et al.*.[22]) The effect of the ASP limits on the event rate vs. m_{χ} plots of Fig. 6 is shown in Fig. 13 where the ruled out areas are marked with big boxes. For $\mu > 0$ the pure photino blob and a few other points are affected, while for $\mu < 0$, virtually every neutralino with $m_{\chi} < 5$ GeV is ruled out. We see that the PETRA and ASP constraints work in a complimentary fashion to rule out most very light ($m_{\chi} \leq 5$ GeV) neutralinos. As new experiments are performed we expect these constraints to strengthen and eventually rule out (or discover) the light neutralino. Unfortunately, we see that current experiments give little information on heavier neutralinos and this situation is unlikely to change in the near future.

VII. Model dependence and other uncertainties

In this section we consider the effect of relaxing a few of the the many simplifying assumptions we made throughout the bulk of this Report. Specifically, we consider the effect of non-degenerate scalar fermion masses and the effect of using the EMC rather than the flavor SU(3) proton spin structure functions.

The assumption of equal mass squarks and sleptons played an important role in producing reasonable cryogenic detector event rates. There are six left chiral squarks, six right chiral squarks and an equal number of sleptons, all of which, in principle, can have different masses. In addition, there can be off-diagonal terms in the mass matrices which result in mixing. These effects have been discussed previously,[1,18] so to limit the possibilities, we will here consider only splitting between the squarks and sleptons, assuming degeneracy among the squarks and among the sleptons themselves. The off-diagonal terms are expected to be small, and the effect of varying squark masses, while possibly

important, is very analogous to squark-slepton splitting. To get an idea of the range of models possible, we surveyed approximately 20 supersymmetric models[35] which used renormalization group techniques to predict the scalar fermion mass splittings. These included "superstring inspired", "heavy top supergravity", and "light top supergravity" models among others. The range of splitting predicted varied substantially from model to model; however, all the models we surveyed were contained within two extreme cases: $M_{\tilde{q}} = M_{\tilde{l}}$ and $M_{\tilde{q}} = 3M_{\tilde{l}}$. We used $M_{\tilde{q}} = M_{\tilde{l}}$ throughout this Report, so we show here the case $M_{\tilde{q}} = 3M_{\tilde{l}}$ to hopefully bracket the effect of scalar fermion splitting.

In Fig. 14 we show the total event rates in a mercury detector for $M_{\tilde{q}} = 3M_{\tilde{l}}$ and the same value of $\tan\beta$ displayed in Fig. 8. The values of $M_{\tilde{q}}$ in Fig. 8 correspond roughly to values of $M_{\tilde{l}}$ in Fig. 14, with $M_{\tilde{q}}$ in Fig. 14 being three time larger. The curves have moved and overall there is a reduction in rate by one to two orders of magnitude. As explained in the introduction this is to be expected. We see that substantial scalar fermion splitting, if it exists, would make neutralino dark matter detection more difficult.

Recent measurements[16] of the spin structure of the proton can be interpreted as giving the surprising result that very little of the spin of the proton is carried by the quarks. While the measurement and interpretation are still controversial, the results, if true, have important implications for neutralino detection. In particular, the matrix element $\langle p|\bar{q}\gamma^{\mu}\gamma_5 q|p\rangle = 2\Delta q\vec{s}_q$ is found to differ substantially from the flavor SU(3) quark model expectations. The effect of this difference is illustrated in Fig. 15 where we show the analogues of Figs. 6b and 7a using EMC rather than flavor SU(3) values for the Δq's. The rates are substantially changed whenever the axial vector term dominates. The scalar term is unaffected. Since the scalar term dominates the rate for mercury, in Fig. 15a we show the axial vector rate only (see Fig. 6b). For fluorine the axial vector term dominates so here we show the total rate (see Fig. 7a). We see that the magnitude and sign of the change caused by using EMC depends sensitively on both the neutralino composition and the nuclear shell model parameterization. Photino-like states (especially the pure photino blobs) seem to be strongly affected, the rate being either strongly enhanced for shell model neutrons like Hg, or suppressed for

shell model protons like F. Note that the positions of the Z^0-squark interference cancellations have moved and that for shell model neutrons there is a general lowering of the rate. The effect of the EMC structure functions on direct detection of neutralinos has also been discussed recently in Ref. 18. This uncertainty in spin structure functions will have to be resolved before accurate determinations of neutralino detection rates can be made.

Finally we mention some other uncertainties and limitations bearing on the results of this Report. First, we note we have ignored the top quark and the Higgs bosons throughout. These particles almost certainly exist in some form, but their masses and properties are unknown. The cross sections and some of our conclusions would change for some values of the top mass. Ellis *et al.*[9] in fact, included a 30 GeV top quark in their original calculations, and this explains some of our differences. The Higgs bosons (there are five in the minimal supersymmetric models) are even more problematic since both masses and mixing parameters are unknown and again, their inclusion could make important changes in our results. Next, we have throughout only considered neutralinos less massive than the Z^0 boson. Heavier neutralinos could exist, but new annihilation channels open up and the problem of ignoring the top quark and Higgs bosons is exacerbated. Certainly, the trend is that detection becomes more difficult as the neutralino mass increases, but a very heavy LSP pushes the masses of the other supersymmetric particles even higher and makes a supersymmetric solution to the hierarchy problem more unlikely. Another limitation is that we considered only the minimal supersymmetric extension of the Standard Model. Although this is the most well studied class of models, many other models have been proposed, and the addition of new particles and couplings can change our predictions drastically. In fact, there may even be particle dark matter whose only interaction with ordinary matter is gravitational. Finally, and most importantly, we have throughout made the assumptions that low-energy supersymmetry exists, and that the neutralino is the LSP.

VIII. Conclusions

In this Report we covered a wide range of topics having to do with the de-

tection of neutralino dark matter. We started by calculating the neutralino annihilation, elastic scattering, and production cross sections and then used these to find the relic abundance of neutralinos and the rate of interaction of galactic neutralinos with a cryogenic detector. New features included additional terms in the cross sections, the inclusion of propagator momenta, and the sign of interference terms. We emphasized that over most of the supersymmetric parameter space a near critical density of neutralinos exists, and that therefore they are likely to constitute a significant fraction ($\Omega_{\tilde{\chi}} \geq .04$) of the galactic halo. This is true whether or not they are, in fact, the dark matter. With regards to direct detection, a new term in the elastic cross section coming from heavy quark loops gives neutralinos a "spin independent" interaction which can be important for heavy materials, and reduces the Z^0-squark negative interference in almost all cases. Pure photinos and pure higgsinos are not affected by the new scalar term.

We then considered the complementary nature of direct detection DM searches and accelerator experiments, showing how results from the PETRA, ASP, and UA1 experiments rule out large areas of parameter space. These constraints in turn affect the detectability of neutralinos. Finally, we considered the effect of non-degenerate squarks and sleptons on our results, showing a reduction in direct detection rates for the most extreme cases of one or two orders of magnitude, and also the effect of the new EMC proton spin structure functions on the rates, showing again a substantial change.

Overall, we found that the neutralino makes a superb particle dark matter candidate, and that the pure photino and pure higgsino special cases usually considered do not represent well the breadth of possibilities. These particles have a chance of being detectable, either directly or in accelerator experiments and we encourage our experimental colleagues to make strong efforts in this direction.

Acknowledgements

We would like to acknowledge very useful conversations with P. Arnold, W. Bardeen, R. Flores, H. Haber, B. Sadoulet, D. Seckel, and M. Turner. This work was supported in part by the DoE (at Chicago). Computing was supported

in part by the DoE and NASA (at Fermilab).

Appendix A

In this appendix we list the complete matrix element, including propagator momenta and non-degenerate squark (or slepton) masses. We also show the initial matrix elements corresponding to the Feynman diagrams in Fig. 1.

For the annihilation process ($\bar{\widetilde{\chi}}\widetilde{\chi} \to \bar{q}q$) labeled by the four-momenta ($p_1 + p_2 \to k_1 + k_2$) the five graphs of Fig. 1 have matrix elements

$$\begin{aligned}
\mathcal{M}_a =& \frac{-2g^2}{(M_{\tilde{q}L}^2 - t)} \bar{u}(k_1)(a\epsilon_j P_L + bP_R)u(p_1)\bar{v}(p_2)(a\epsilon_i P_R + bP_L)v(k_2) \\
\mathcal{M}_b =& \frac{-2g^2}{(M_{\tilde{q}R}^2 - t)} \bar{u}(k_1)(-aP_R + \epsilon_j cP_L)u(p_1)\bar{v}(p_2)(-aP_L + \epsilon_i cP_R)v(k_2) \\
\mathcal{M}_c =& \frac{-2g^2}{(M_{\tilde{q}L}^2 - u)} \bar{v}(p_2)(aP_L + \epsilon_j bP_R)v(k_1)\bar{u}(k_2)(aP_R + \epsilon_j bP_L)u(p_1) \qquad (A1) \\
\mathcal{M}_d =& \frac{-2g^2}{(M_{\tilde{q}R}^2 - u)} \bar{v}(p_2)(-\epsilon_j aP_R + cP_L)v(k_1)\bar{u}(k_2)(-\epsilon_i aP_L + cP_R)u(p_1) \\
\mathcal{M}_z =& \frac{-g^2(Z_{13}^2 - Z_{14}^2)}{2\cos^2\theta_w(m_Z^2 - s)} \bar{v}(p_2)\gamma^\mu\gamma_5 u(p_1)\bar{u}(k_1)\gamma_\mu(c_L P_L + c_R P_R)v(k_2),
\end{aligned}$$

where ϵ_i is the sign of the neutralino mass eigenvalue and the other symbols are defined in Sec. II.

The total matrix element is $\mathcal{M} = \mathcal{M}_z + \mathcal{M}_c + \mathcal{M}_d - \mathcal{M}_a - \mathcal{M}_b$. The total matrix element squared is the sum of the following terms.

$$\begin{aligned}
|\mathcal{M}_a|^2 =& \frac{16g^4}{(M_{\tilde{q}L}^2 - t)^2}\Big[(a^2 + b^2)^2(k_1p_1)(k_2p_2) + 4a^2b^2{m_q}^2{m_X}^2 \\
&+ 2m_q m_X ab(a^2 + b^2)\epsilon\left((k_1p_1) + (k_2p_2)\right)\Big] \\
|\mathcal{M}_b|^2 =& \frac{16g^4}{(M_{\tilde{q}R}^2 - t)^2}\Big[(a^2 + c^2)^2(k_1p_1)(k_2p_2) + 4a^2c^2{m_q}^2{m_X}^2
\end{aligned}$$

$$- 2m_q m_X ac(a^2+c^2)\epsilon\big((k_1p_1)(k_2p_2)\big)\Big] \qquad (A2)$$

$$|\mathcal{M}_c|^2 = \frac{16g^4}{(M_{\tilde{q}R}^2-u)^2}\Big[(a^2+b^2)^2(k_1p_2)(k_2p_1) + 4a^2b^2m_X^2{m_q}^2 + 2m_q m_X ab(a^2+b^2)\epsilon\big((k_1p_2)+(k_2p_1)\big)\Big]$$

$$|\mathcal{M}_d|^2 = \frac{16g^4}{(M_{\tilde{q}R}^2-u)^2}\Big[(a^2+c^2)^2(k_1p_2)(k_2p_1) + 4a^2c^2{m_q}^2m_X^2 - 2m_q m_X ac(a^2+c^2)\epsilon\big((k_1p_2)+(k_2p_1)\big)\Big]$$

$$|\mathcal{M}_z|^2 = \frac{16g^4(Z_{13}^2-Z_{14}^2)^2}{\cos^4\theta_w(m_Z^2-s)^2}\Big[\frac{1}{4}(c_L^2+c_R^2)\big((k_1p_2)(k_2p_1)+(k_1p_1)(k_2p_2)-m_X^2(k_1k_2)\big) + \frac{1}{2}c_Lc_R{m_q}^2\big((p_1p_2)-2m_X^2\big)\Big]$$

$$2Re\mathcal{M}_a\mathcal{M}_b^* = \frac{32g^4}{(M_{\tilde{q}L}^2-t)(M_{\tilde{q}R}^2-t)}\big[a(c-b)(k_1p_1)+m_qm_X\epsilon(bc-a^2)\big] \times \big[a(c-b)(k_2p_2)+m_qm_X\epsilon(bc-a^2)\big]$$

$$2Re\mathcal{M}_a\mathcal{M}_c^* = \frac{16g^4}{(M_{\tilde{q}L}-t)(M_{\tilde{q}L}-u)}\Big\{2a^2b^2\Big[(p_1k_2)(p_2k_1) + (k_1p_1)(k_2p_2) - (k_1k_2)(p_1p_2) + {m_q}^2m_X^2 + {m_q}^2(p_1p_2)\Big] + (a^4+b^4)m_X^2(k_1k_2) + m_qm_Xab\epsilon(a^2+b^2)\big[(p_2k_1)+(p_1k_2)+(p_1k_1)+(p_2k_2)\big]\Big\}$$

$$2Re\mathcal{M}_a\mathcal{M}_d^* = \frac{16g^4}{(M_{\tilde{q}L}-t)(M_{\tilde{q}R}-u)}\Big\{-2a^2bc\Big[(p_1k_2)(p_2k_1)+(k_1p_1)(k_2p_2) - (k_1k_2)(p_1p_2)+{m_q}^2m_X^2\Big] + a^2(b^2+c^2)m_X^2(k_1k_2) + {m_q}^2(a^4+b^2c^2)(p_1p_2) + m_qm_Xa\epsilon\big[b(a^2+c^2)\big((p_2k_1)+(p_1k_2)\big) - c(a^2+b^2)\big((p_1k_1)+(p_2k_2)\big)\big]\Big\}$$

$$
\begin{aligned}
2Re\mathcal{M}_b\mathcal{M}_c^* =& \frac{16g^4}{(M_{\tilde{q}R}-t)(M_{\tilde{q}L}-u)}\Big\{-2a^2bc\Big[(p_1k_2)(p_2k_1)+(k_1p_1)(k_2p_2)\\
&-(k_1k_2)(p_1p_2)+{m_q}^2m_X^2\Big]\\
&+a^2(b^2+c^2)m_X^2(k_1k_2)+{m_q}^2(a^4+b^2c^2)(p_1p_2)\\
&+m_qm_Xa\epsilon\big[-c(a^2+b^2)\big((p_2k_1)+(p_1k_2)\big)+b(a^2+c^2)\big((p_1k_1)+(p_2k_2)\big)\big]\Big\}\\
2Re\mathcal{M}_b\mathcal{M}_d^* =& \frac{16g^4}{(M_{\tilde{q}R}-t)(M_{\tilde{q}R}-u)}\Big\{2a^2c^2\Big[(p_1k_2)(p_2k_1)+(k_1p_1)(k_2p_2)\\
&-(k_1k_2)(p_1p_2)+{m_q}^2m_X^2+{m_q}^2(p_1p_2)\Big]\\
&+(a^4+c^4)m_X^2(k_1k_2)\\
&-m_qm_Xac\epsilon(a^2+c^2)\big[(p_2k_1)+(p_1k_2)+(p_1k_1)+(p_2k_2)\big]\Big\}\\
2Re\mathcal{M}_c\mathcal{M}_d^* =& \frac{32g^4}{(M_{\tilde{q}L}^2-u)(M_{\tilde{q}R}^2-u)}\big[a(c-b)(k_1p_2)+m_qm_X\epsilon(bc-a^2)\big]\\
&\times\big[a(c-b)(k_2p_1)+m_qm_X\epsilon(bc-a^2)\big]\\
2Re\mathcal{M}_a\mathcal{M}_z^* =& \frac{8g^4(Z_{13}^2-Z_{14}^2)}{\cos^2\theta_w(m_Z^2-s)(M_{\tilde{q}L}^2-t)}\Big\{2(b^2c_L-a^2c_R)(k_1p_1)(k_2p_2)\\
&+2(a^2c_L-b^2c_R){m_q}^2m_X^2-(a^2c_L-b^2c_R){m_q}^2(p_1p_2)\\
&-(b^2c_L-a^2c_R)m_X^2(k_1k_2)\\
&+ab\epsilon m_qm_X(c_R-c_L)\big[(p_1k_2)+(p_2k_1)-2(k_1p_1)-2(k_2p_2)\big]\Big\}\\
2Re\mathcal{M}_b\mathcal{M}_z^* =& \frac{8g^4(Z_{13}^2-Z_{14}^2)}{\cos^2\theta_w(m_Z^2-s)(M_{\tilde{q}R}^2-t)}\Big\{2(a^2c_L-c^2c_R)(k_1p_1)(k_2p_2)\\
&+2(c^2c_L-a^2c_R){m_q}^2m_X^2-(c^2c_L-a^2c_R){m_q}^2(p_1p_2)\\
&-(a^2c_L-c^2c_R)m_X^2(k_1k_2)\\
&+ac\epsilon m_qm_X(c_R-c_L)\big[(-p_1k_2)-(p_2k_1)+2(k_1p_1)+2(k_2p_2)\big]\Big\}\\
2Re\mathcal{M}_c\mathcal{M}_z^* =& \frac{8g^4(Z_{13}^2-Z_{14}^2)}{\cos^2\theta_w(m_Z^2-s)(M_{\tilde{q}L}^2-u)}\Big\{2(a^2c_R-b^2c_L)(k_1p_2)(k_2p_1)\\
&+2(b^2c_R-a^2c_L){m_q}^2m_X^2-(b^2c_R-a^2c_L){m_q}^2(p_1p_2)
\end{aligned}
$$

$$
\begin{aligned}
&- (a^2 c_R - b^2 c_L) m_X^2 (k_1 k_2) \\
&+ ab\epsilon m_q m_X (c_R - c_L)\big[2(p_1 k_2) + 2(p_2 k_1) - (k_1 p_1) - (k_2 p_2)\big]\Big\},
\end{aligned}
$$

$$
\begin{aligned}
2Re\mathcal{M}_d \mathcal{M}_z^* = &\frac{8g^4(Z_{13}^2 - Z_{14}^2)}{\cos^2\theta_w (m_Z^2 - s)(M_{\tilde{q}R}^2 - u)}\Big\{2(c^2 c_R - a^2 c_L)(k_1 p_2)(k_2 p_1) \\
&+ 2(a^2 c_R - c^2 c_L) m_q{}^2 m_X^2 - (a^2 c_R - c^2 c_L) m_q{}^2 (p_1 p_2) \\
&- (c^2 c_R - a^2 c_L) m_X^2 (k_1 k_2) \\
&+ ac\epsilon m_q m_X (c_R - c_L)\big[-2(p_1 k_2) - 2(p_2 k_1) + (k_1 p_1) + (k_2 p_2)\big]\Big\},
\end{aligned}
$$

where all symbols were defined in Sec. II.

REFERENCES

1. M. W. Goodman and E. Witten, *Phys. Rev* **D31** (1985) 3059; I. Wasserman, *Phys. Rev.* **D33** (1986)2071.
2. A. K. Drukier, K. Freese and D. N. Spergel, *Phys. Rev.* **D33** (1986) 3495.
3. K. Freese, J. Frieman and A. Gould, SLAC Report No. SLAC-PUB-4427, 1987 (to be published).
4. K. Griest, *Phys. Rev.* **D37** (1988) 2703.
5. J. Silk, K. A. Olive and M. Srednicki, *Phys. Rev. Lett.* **53** (1985) 624; T. K. Gaisser, G. Steigman and S. Tilav, *Phys. Rev.* **D34** (1986) 2206; J. S. Hagelin, K. W. Ng and K. A. Olive, *Phys. Lett.* **180B** (1987) 375.
6. L. M. Krauss, M. Srednicki and F. Wilczek, *Phys. Rev.* **D33** (1986) 2079; K. Freese, *Phys. Lett.* **167B** (1986) 295.
7. H. E. Haber and G. L. Kane, *Phys. Rep.* **117** (1985) 75.
8. J. F. Gunion and H. E. Haber, *Nucl. Phys.* **B272** (1986) 1.
9. J. Ellis, J. S. Hagelin, D. V. Nanopoulos, K. A. Olive and M. Srednicki, *Nucl. Phys.* **B238** (1984) 453.
10. Other possible LSP candidates include the sneutrino and gravitino. They are more difficult to consistently arrange as dark matter and we will not consider them here.
11. M. A. Shifman, A. I. Vainshtein and V. I. Zakharov, *Phys. Lett.* **78B** (1978) 443; A. I. Vainshtein, V. I. Zakharov and M. A. Shifman, *Sov. Phys. Usp.* **23** (1980) 429.
12. K. Griest and B. Sadoulet, *Model Independence of Constrants on Particle Dark Matter,* 1987 (unpublished).
13. C. Albajar *et al.*, *Phys. Lett.* **198B** (1987) 261.
14. W. Bartel *et al.*, *Z. Phys.* **C29** (1985) 505; H. -J. Behrend *et al.*, *Z. Phys.* **C35** (1987) 181.
15. C. Hearty *et al.*, *Phys. Rev. Lett.* **58** (1987) 1711; G. Bartha *et al.*, *Phys. Rev. Lett.* **56** (1986) 685.

16. J. Ashman, *et al.*, CERN Report No. CERN-EP/87-230, 1987 (to be published).

17. We follow the convention in which H_1 gives mass to the down type quarks and H_2 gives mass to the up type. This is the opposite of the Ellis *et al.*[9] convention, implying $Z_{13} \leftrightarrow Z_{14}$ and $\tan\beta \rightarrow v_1/v_2$. Also, our μ corresponds to their $-\epsilon$.

18. J. Ellis and R. A. Flores, CERN Report No. CERN-TH.4911/87 1988 (to be published).

19. G. L. Kane and I. Kani, *Nucl. Phys.* **B277** (1986) 525; B. A. Campbell, *et al.*, *Phys. Lett.* **173B** (1986) 270.

20. R. Watkins, private communication.

21. P. Fayet, *Phys. Lett.* **117B** (1982) 461; K. Grassie and P. N. Pandita, *Phys. Rev.* **D30** (1984) 22.

22. M. Dress, C. S. Kim and X. Tata, *Phys. Rev.* **D37** (1988) 784.

23. J. Ellis, R. A. Flores and S. Ritz, *Phys. Lett.* **198B** (1987) 393.

24. A Bayesian analysis gives instead $\sigma(e^+e^- \rightarrow \tilde{\bar{\chi}}\tilde{\chi}\gamma) \leq .046$ pb, but both statistical methods have problems so we use the simpler one.

25. C. Hearty, private communication.

26. H. -J. Behrend *et al.*, *Phys. Lett.* **B176** (1986) 247.

27. A. de-Shalit and I. Talmi, *Nuclear Shell Theory* (Academic Press, New York, 1963).

28. S. Raby and G. B. West, *Phys. Lett.* **202B** (1988) 47.

29. B. W. Lee and S. Weinberg, *Phys. Rev. Lett.* **39** (1977) 165; Ya. B. Zeldovich, L. B. Okun and S. Pikel'ner, *Sov. Phys. Uspelchi* **8** (1966) 702.

30. K. Griest and D. Seckel, *Nucl. Phys.* **B283** (1987) 681; erratum, *ibid.*, **B296** (1988) 1034.

31. K. Griest, Ph. D thesis, University of California, Santa Cruz, 1987 (SCIPP 87/92).

32. E. W. Kolb and K. A. Olive, *Phys. Rev.* **D33** (1986) 1202; R. J. Scherrer and M. S. Turner, *Phys. Rev.* **D33** (1986) 1585.

33. D. O. Caldwell *et al.*, University of California, Santa Barbara Report No. UCSB-HEP-87-13 (to be published); S. P. Ahlen *et al.*, *Phys. Lett.* **B195** (1987) 603.

34. J. Grivaz, published in Moriand 1987:Leptons:115 (LAL Report No. 87-20).

35. L. E. Ibanez and J. Mas, *Nucl. Phys.* **B286** (1987) 107; L. E. Ibanez, C. Lopez and C. Munoz, *Nucl. Phys.* **B256** (1985) 218; L. E. Ibanez and C. Lopez, *Nucl. Phys.* **B233** (1984) 511.

36. K. Griest, Fermilab Report No. FERMILAB-Pub-88/52-A, 1988 (to be published).

Figure Captions

1. Feynman diagrams contributing to neutralino ($\widetilde{\chi}$) interaction with quarks or leptons (q). The first diagram shows Z^0 exchange while the last four show left and right chiral squark (or slepton) exchange.

2. Relic abundances of neutralinos vs. the neutralino mass. Each "x" shows a different supersymmetric model. The horizontal line denotes critical density ($\Omega = 1$) for $h = \frac{1}{2}$. Supersymmetric models with parameters in the wide range $0 \leq M \leq 1$ TeV and $0 \leq \mu \leq 1$ TeV are shown for several values of squark mass $M_{\tilde{q}}$ and $\tan\beta$.

3. Contours of $\Omega_{\tilde{\chi}} h^2 = \frac{1}{4}$ in the M, μ plane for various values of $M_{\tilde{q}}$ and $\tan\beta$. Figs. 3a and 3b show the $\mu > 0$ case while Figs. 3c and 3d show $\mu < 0$. Solid lines indicate $\tan\beta = \frac{3}{4}$, dashed lines indicate $\tan\beta = 2$ and dot-dashed lines indicate $\tan\beta = \frac{1}{4}$.

4. Consistency constraint: contours of $m_X = m_{\tilde{\chi}_\pm}$ in the M, μ plane for various values of $M_{\tilde{q}}$ and $\tan\beta$, where $m_{\tilde{\chi}_\pm}$ is the mass of the lightest chargino. The areas between the contours are inconsistent with the neutralino as LSP. Fig. 4a shows the $\Omega_{\tilde{\chi}} h^2 = \frac{1}{4}$ contour (solid lines) being cut by the $m_X = m_{\tilde{\chi}_\pm}$ contour (dashed lines) for $M_{\tilde{q}} = 50$ GeV and $\tan\beta = \frac{1}{2}$. Fig. 4b shows contours for $M_{\tilde{q}} = 100$ GeV and several values of $\tan\beta$. See Fig. 3 caption for the code for lines.

5. Coherence loss factor η_c as a function of neutralino and nuclei mass. The various lines are labeled on the right by the nuclei mass in GeV.

6. Event rates in a cryogenic detector made of mercury as a function of neutralino mass. All points correspond to $\Omega_{\tilde{\chi}} h^2 = \frac{1}{4}$ for $\tan\beta = .25$, $.75$, or 2 and $M_{\tilde{q}} = 50$ or 125 GeV. Lines in Figs. 6a,d are labeled by $\tan\beta$. The solid lines indicate $M_{\tilde{q}} = 50$ GeV while the dashed lines indicate $M_{\tilde{q}} = 125$ GeV. Figs. 6a,b,c show the $\mu > 0$ case while Figs. 6d,e,f show the $\mu < 0$ case.

Figs. 6a,d show the total rate, Figs. 6b,e show the contribution from the axial vector term alone and Figs. 6c,f show the new scalar term contribution alone.

7. Same as Fig. 6 for detectors made of fluorine and thallium. Only the $\mu > 0$ cases are shown.

8. Effect of varying squark mass: Event rates in a thallium detector as a function of neutralino mass for $\tan\beta = \frac{1}{2}$ and $M_{\tilde{q}} = 50$, 60, 75, 100, 125, 150, and 200 GeV. The lines and "pure photino blobs" are labeled with the squark mass in GeV. For $\mu > 0$ (Fig. 8a) no blobs were found for $M_{\tilde{q}} \geq 125$ geV, and for $\mu < 0$ (Fig. 8b) no blob was found for $M_{\tilde{q}} = 200$ GeV.

9. Effect of varying $\tan\beta$: Event rates in a thallium detector as a function of neutralino mass for $M_{\tilde{q}} = 50$ and $\tan\beta = .25$, .33, .75, 1, 3. The lines are labeled by $\tan\beta$.

10. Effect of propagator momenta for the pure photino. For each value of photino mass m_χ, $M_{\tilde{q}}$ is found so that $\Omega_{\tilde{\chi}} h^2 = \frac{1}{4}$ and the corresponding event rate in a fluorine cryogenic detector displayed. Curves show the effect of propagator momenta both in the annihilation cross section and in the elastic scattering cross section. Flavor SU(3) spin structure functions were used.

11. PETRA constraint. Contours of $m_{\tilde{\chi}^\pm} = 23$ GeV in the M, μ plane are shown for several values of $\tan\beta$. Fig. 11a shows the $\mu > 0$ case where the areas *between* the contours are ruled out due to $m_{\tilde{\chi}^\pm} < 23$ GeV. Fig. 11b shows the $\mu < 0$ case where the areas *outside* the contours are ruled out.

12. ASP constraint. Contours of $\sigma_{ASP} = .03$ pb (see text) in the M, μ plane are shown for $M_{\tilde{q}} = 50$ and several values of $\tan\beta$. The code for the lines is the same as in Fig. 3. The areas below the long contours and inside the "wedges" at the far right are ruled out. Only the $\mu > 0$ case is shown; the $\mu < 0$ case is very similar except the horizontal contours continue straight

across to $\mu = 1$ TeV and there are no "wedges". There are no solutions for $M_{\tilde{q}} = 125$ GeV and so no constraints exist for that case.

13. Effect of PETRA and ASP constraints. Event rates in a mercury detector as a function of the neutralino mass (same as Figs. 6a,d) with areas ruled out by the PETRA and ASP constraints marked. Fig. 13a shows the $\mu > 0$ case while Fig. 13b shows the $\mu < 0$ case. Areas ruled out by PETRA are marked with "x"'s and areas ruled out by ASP are marked with large boxes.

14. Effect of non-degenerate squarks and sleptons. Event rates in a thallium detector as a function of the neutralino mass with $M_{\tilde{q}} = 3M_{\tilde{l}}$ instead of $M_{\tilde{q}} = M_{\tilde{l}}$ (see Fig. 8). Lines and blobs are labeled by the value of the squark mass in GeV. In comparing with Fig. 8 the relevant mass is actually the selectron mass; one third of the labeled mass. Fig. 14a shows the $\mu > 0$ case while Fig. 14b shows the $\mu < 0$ case.

15. Effect of EMC structure functions. Same as Fig. 6b (15a) and Fig. 7a (15b) with EMC rather than flavor SU(3) spin dependent structure functions.

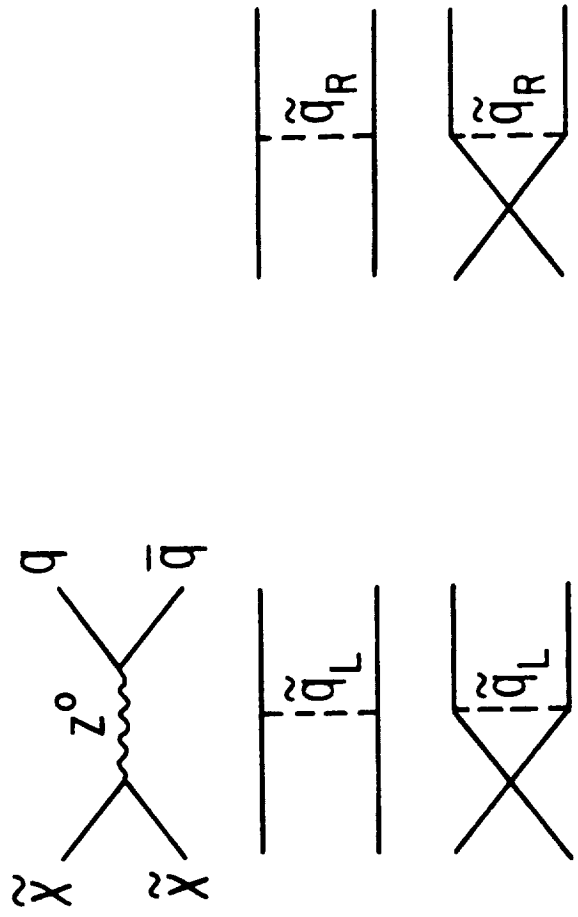

Fig. 1

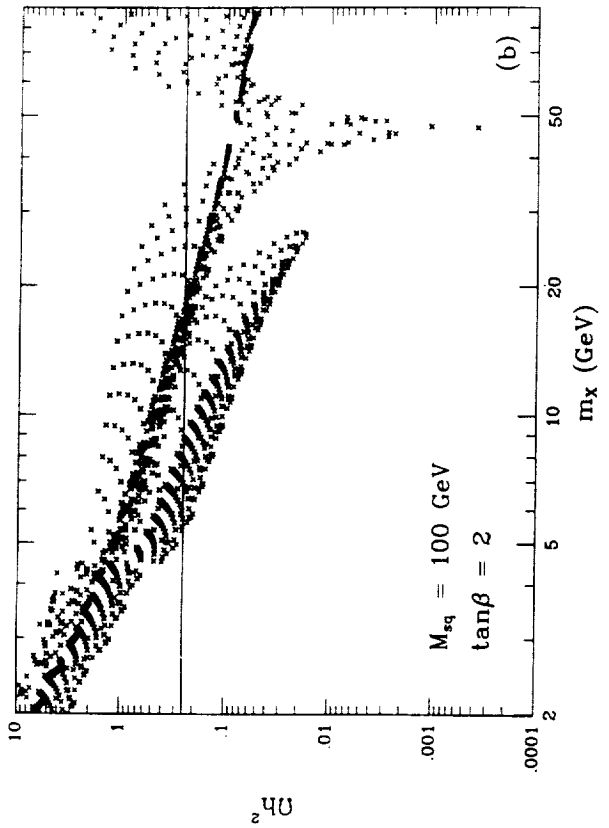

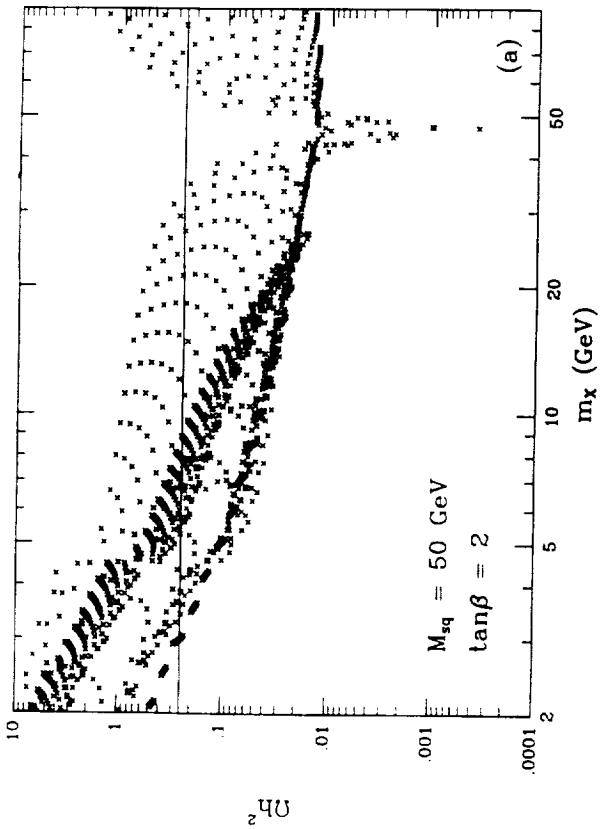

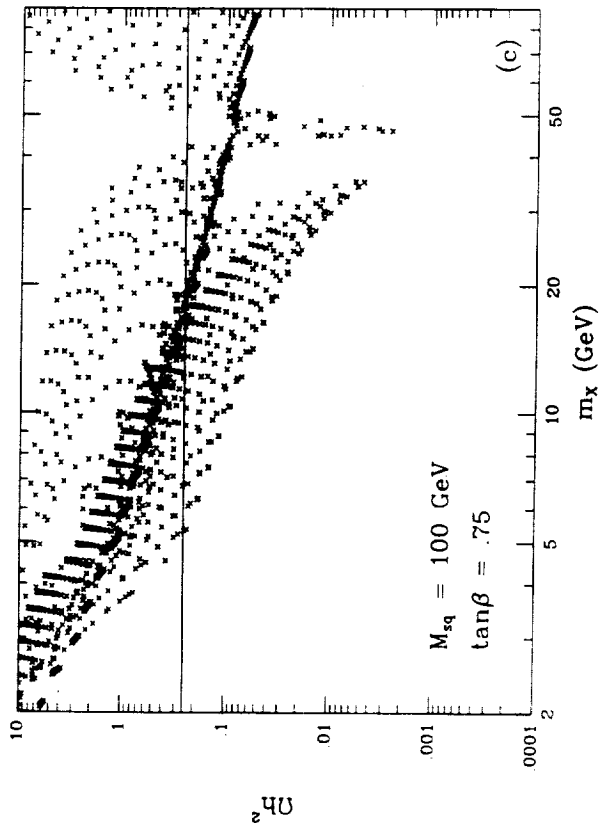

Fig. 2

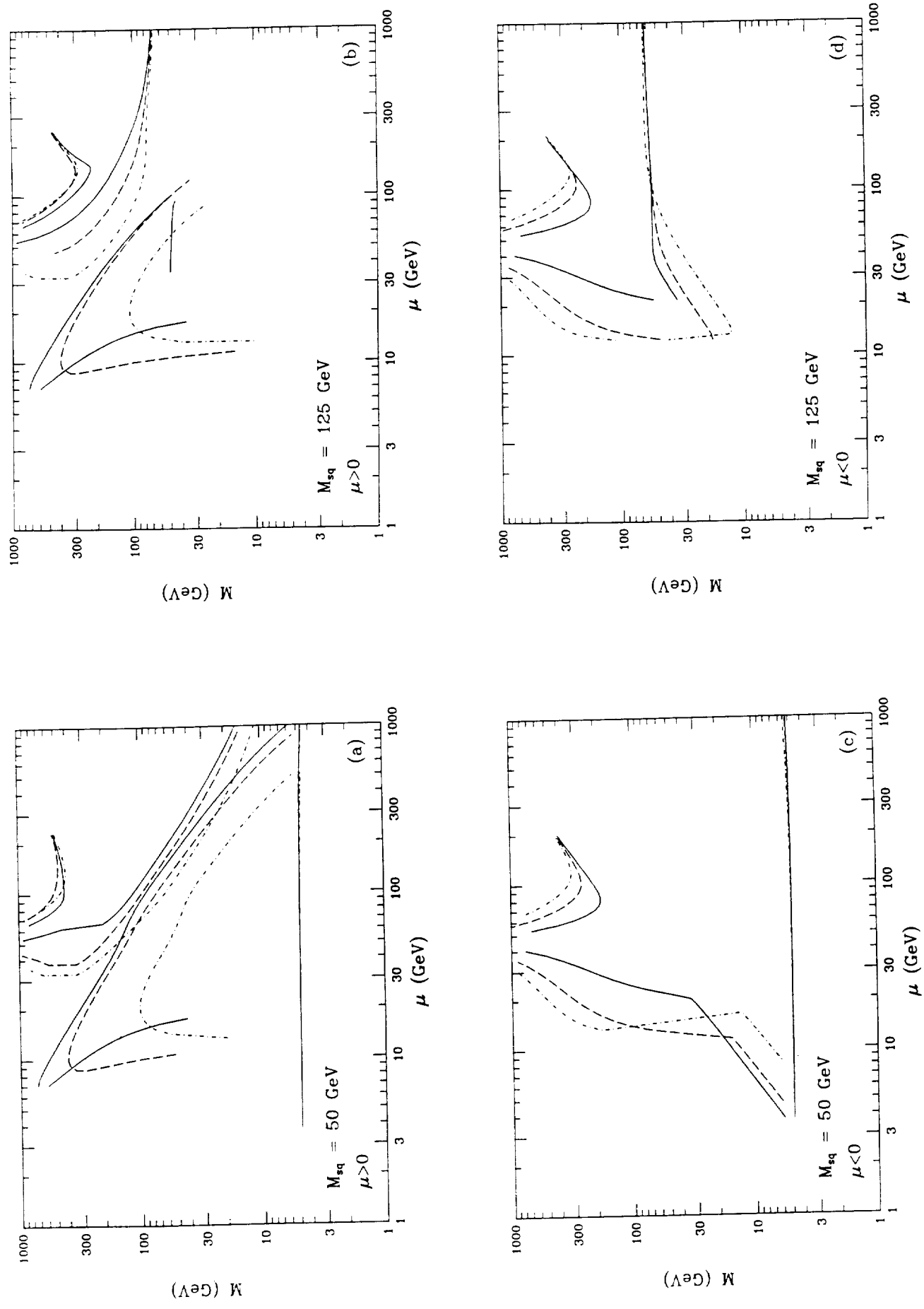

Fig. 2

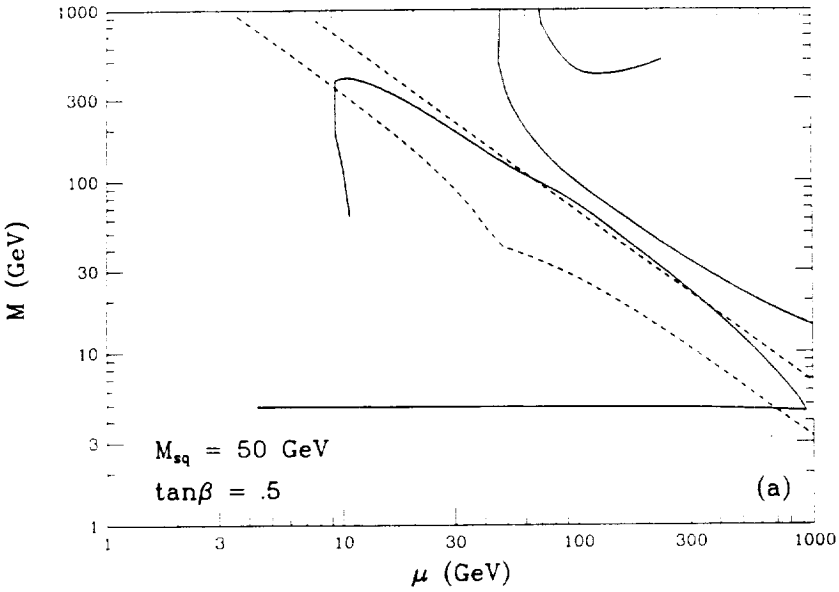

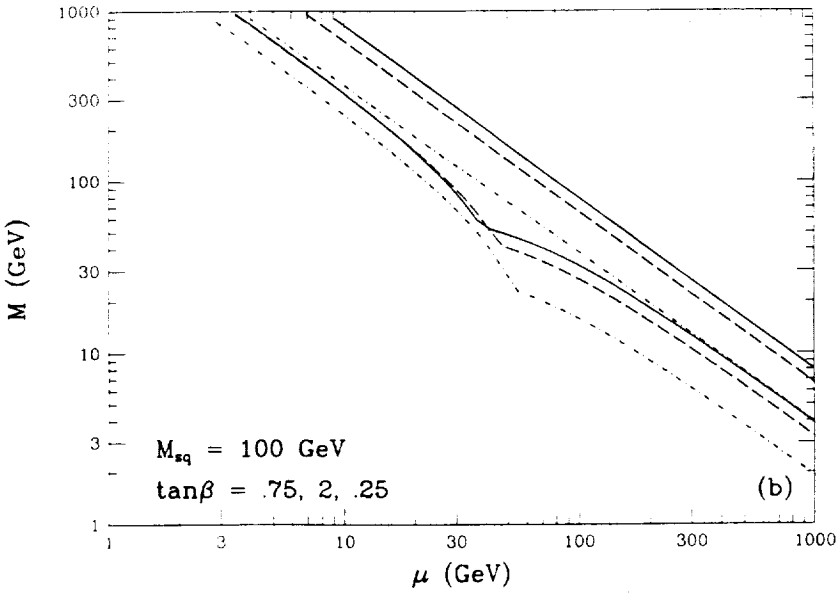

Fig. 4

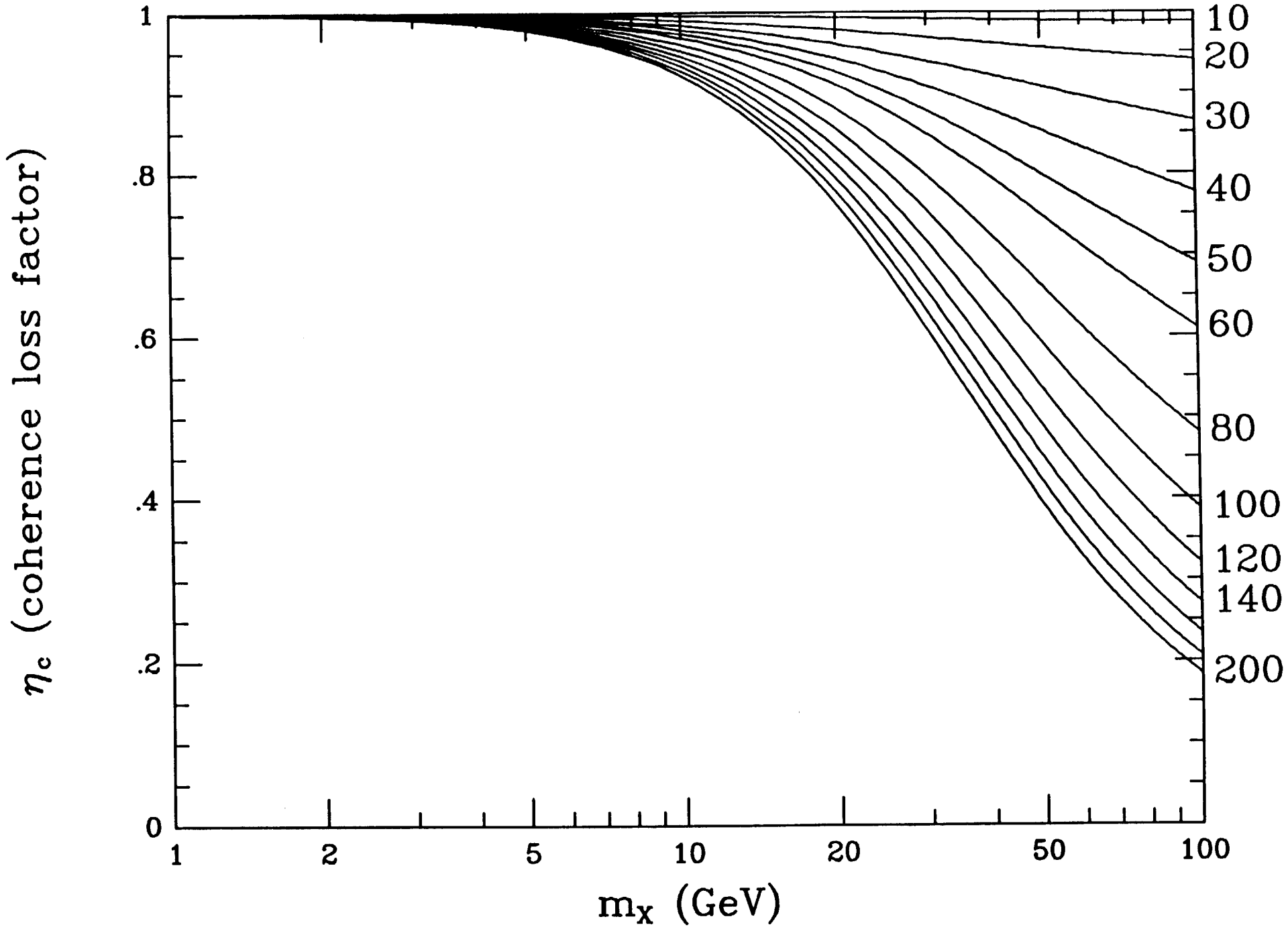
η_c (coherence loss factor)
1
.8
.6
.4
.2
0
1
2
5
10
20
50
100
m_X (GeV)
10
20
30
40
50
60
80
100
120
140
200

Fig.5

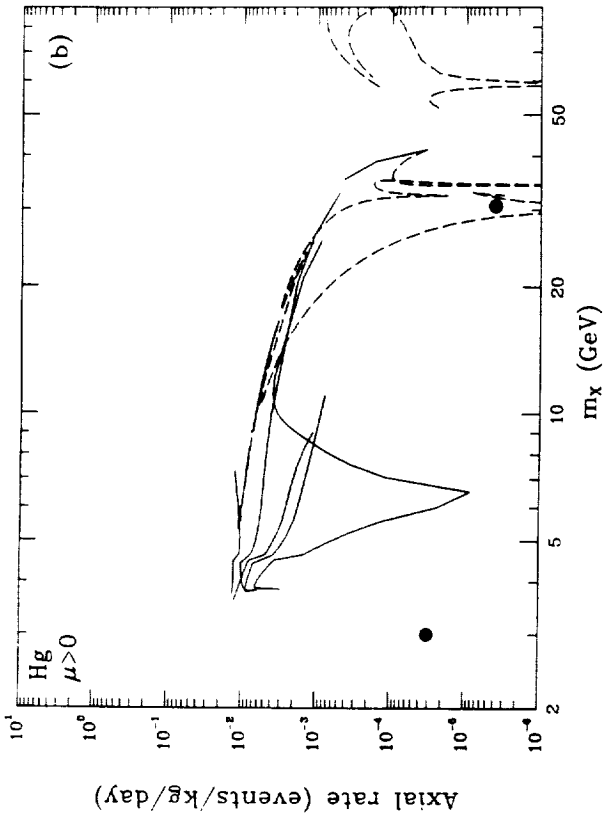

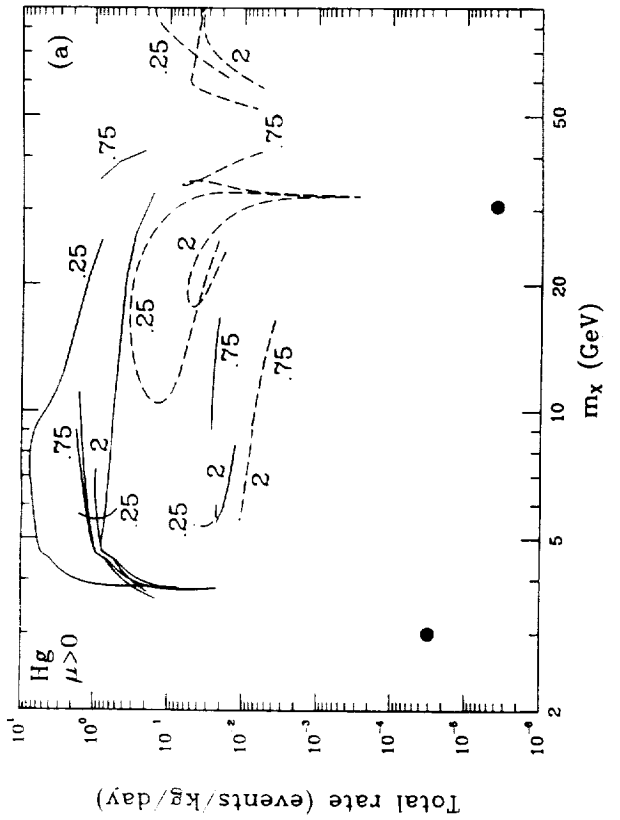

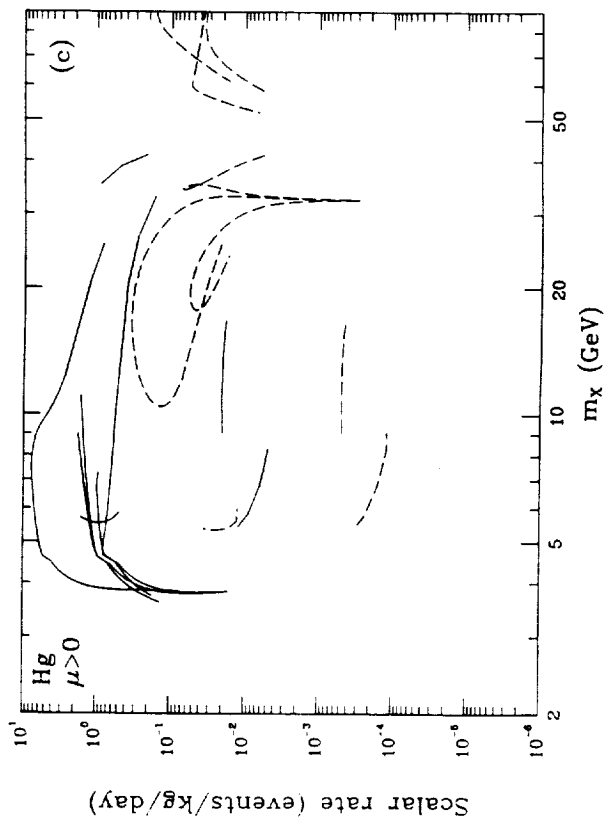

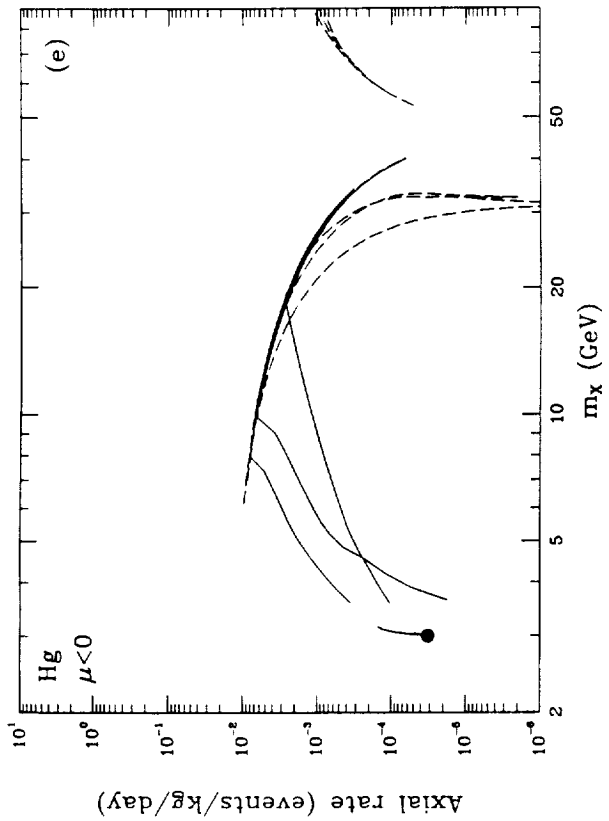

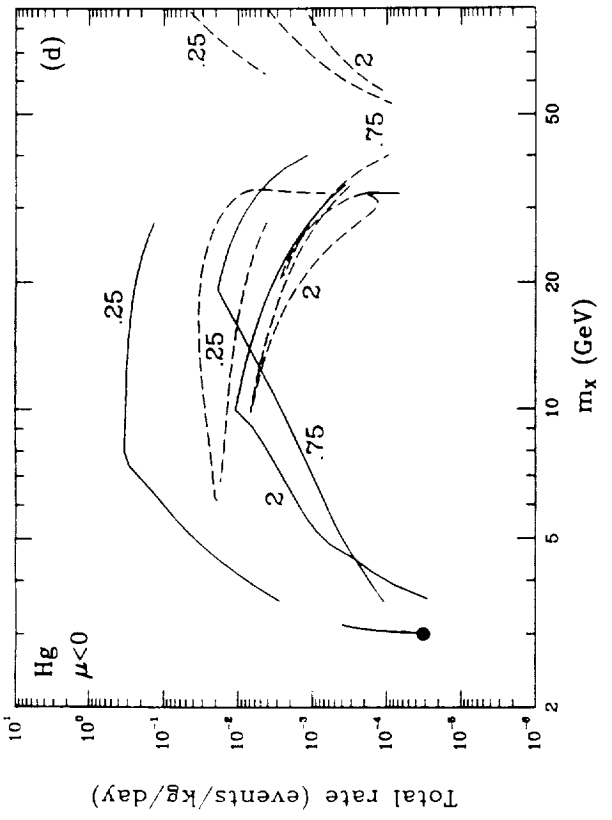

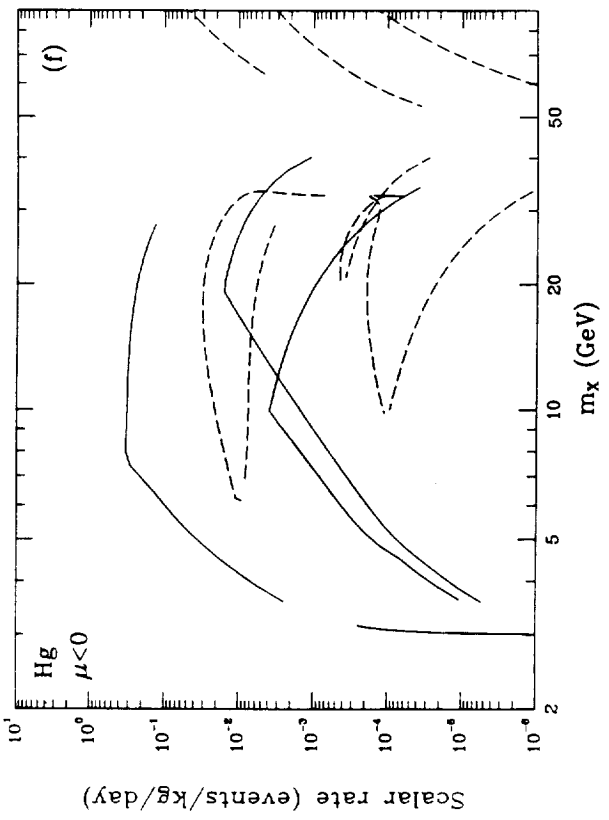

Fig. 8a,b

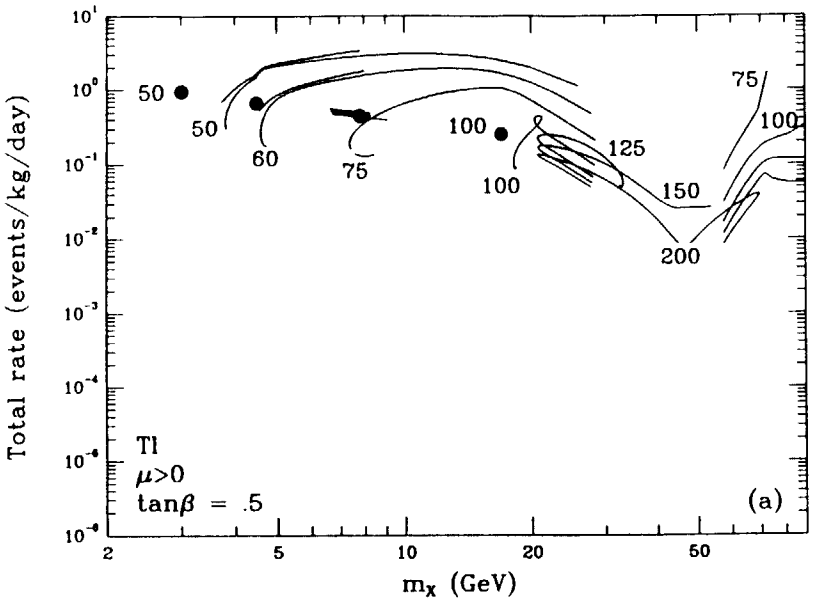

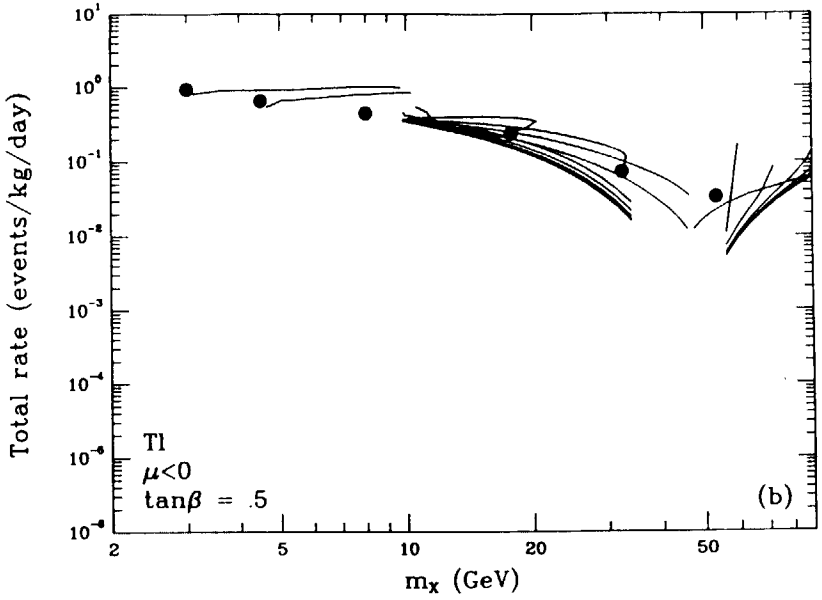

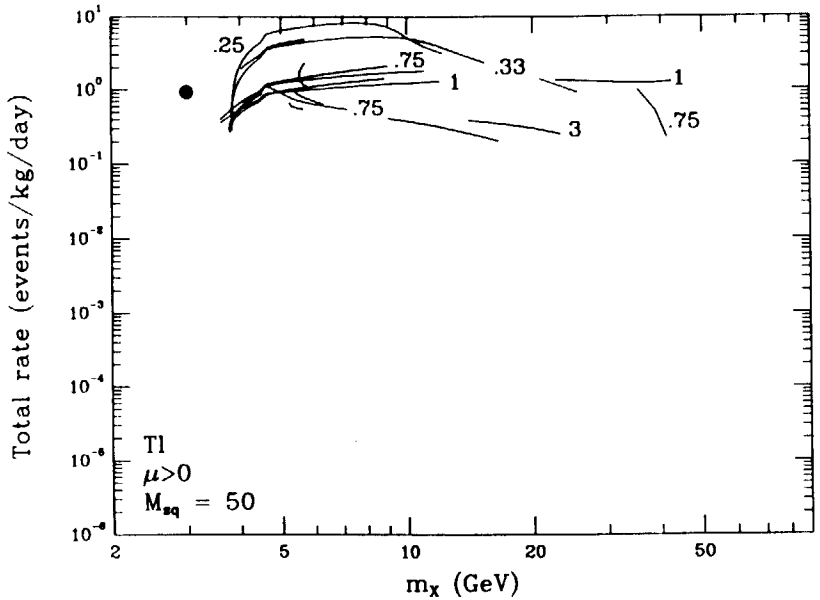

Fig. 9

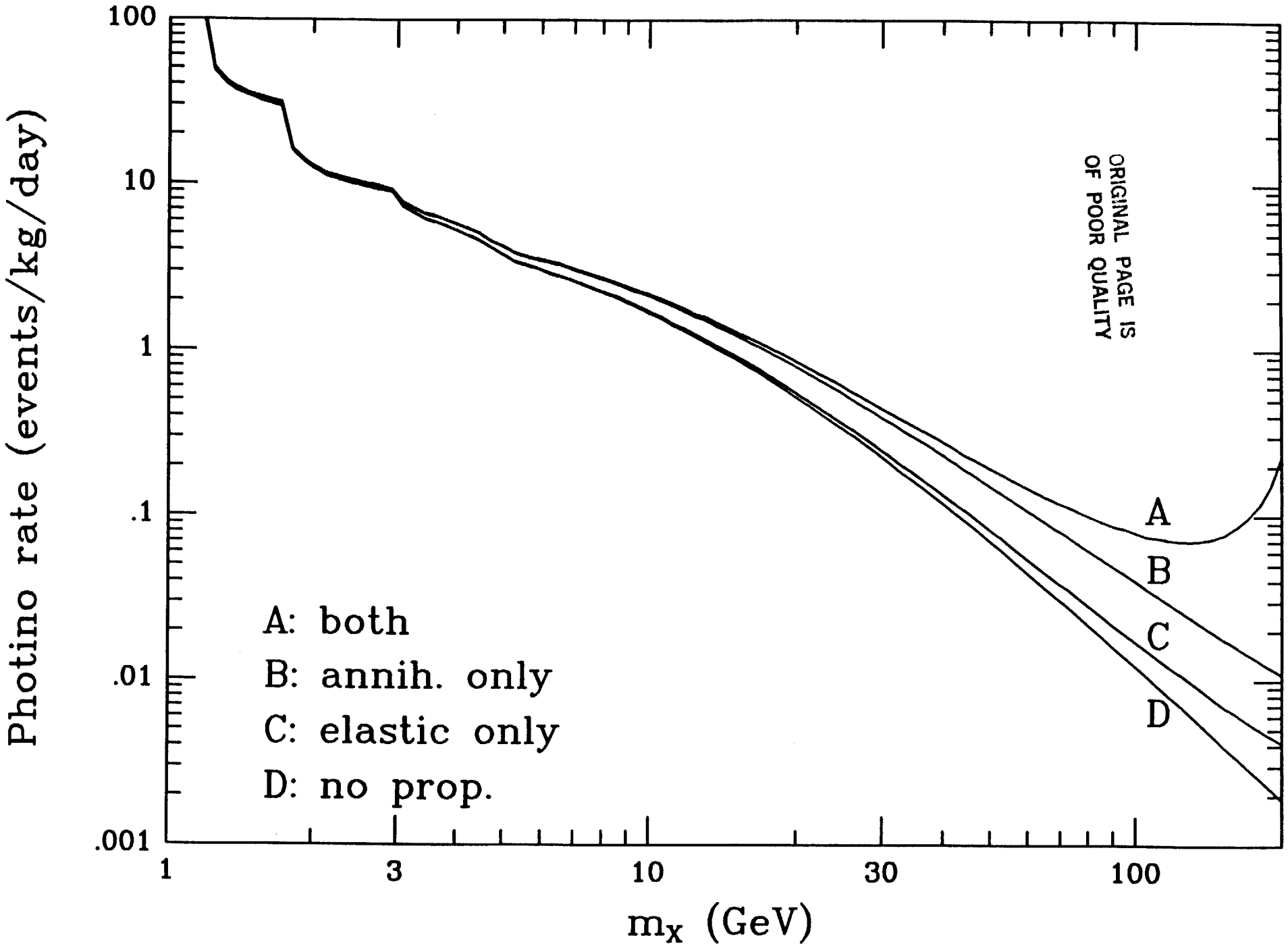
Photino rate (events/kg/day)
100
10
1
.1
.01
.001
1
3
10
30
100
m_X (GeV)
A: both
B: annih. only
C: elastic only
D: no prop.
A
B
C
D
ORIGINAL PAGE IS
OF POOR QUALITY

Fig. 10

Fig. 11a,b

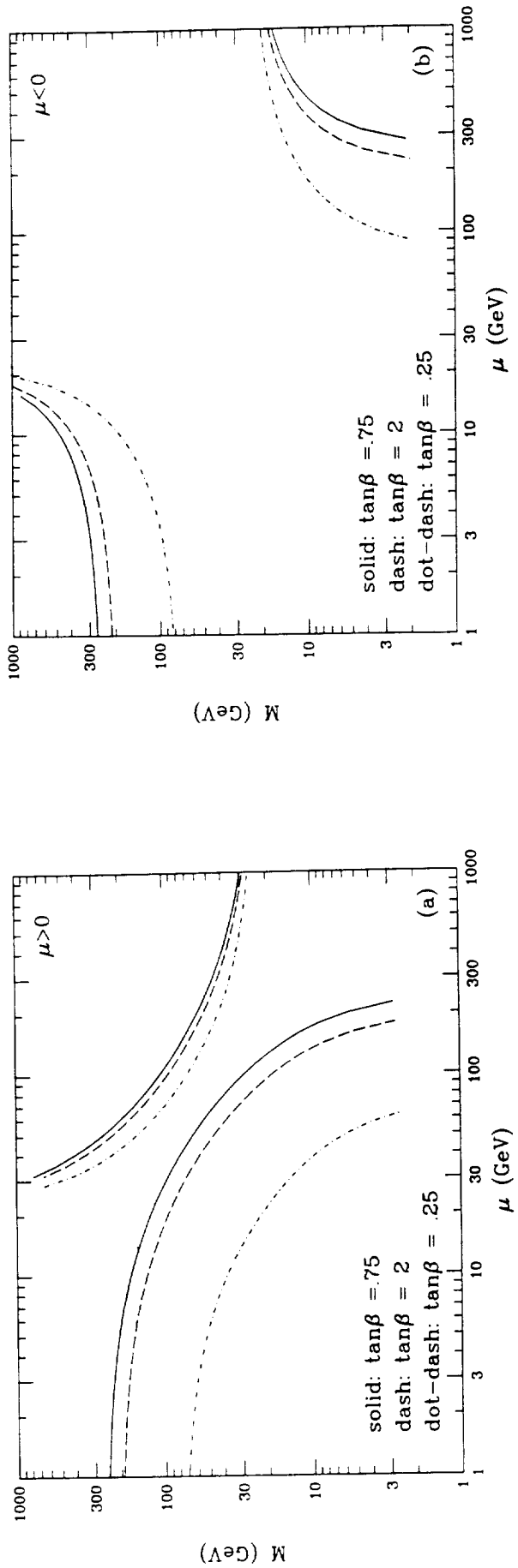

Fig. 12

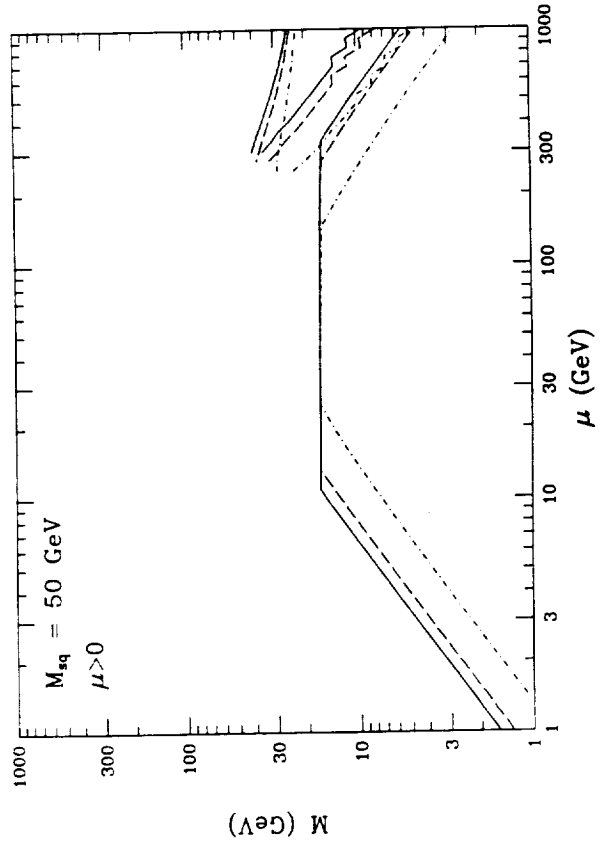

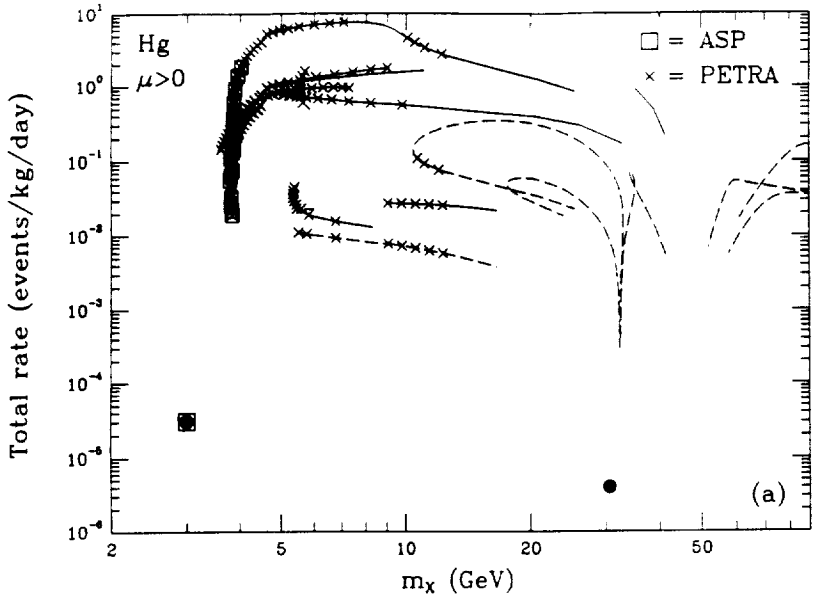

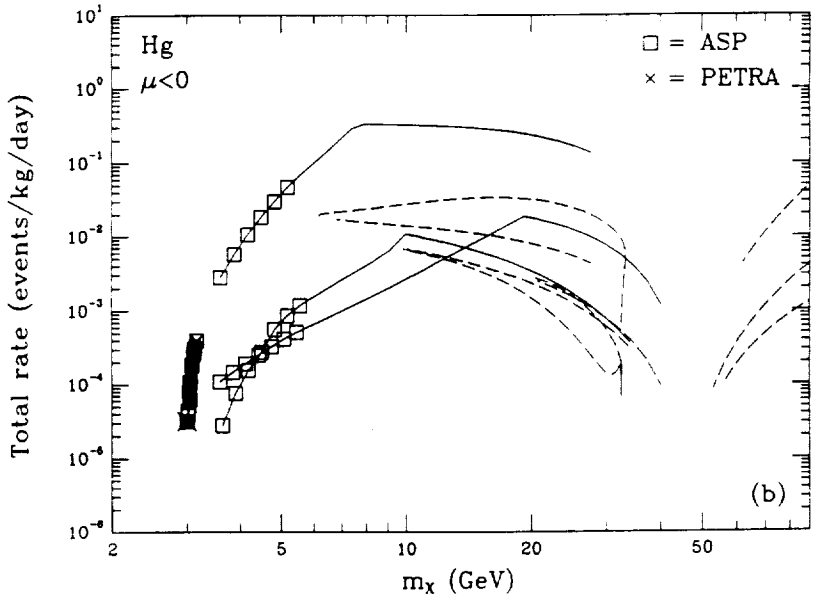

Fig 13

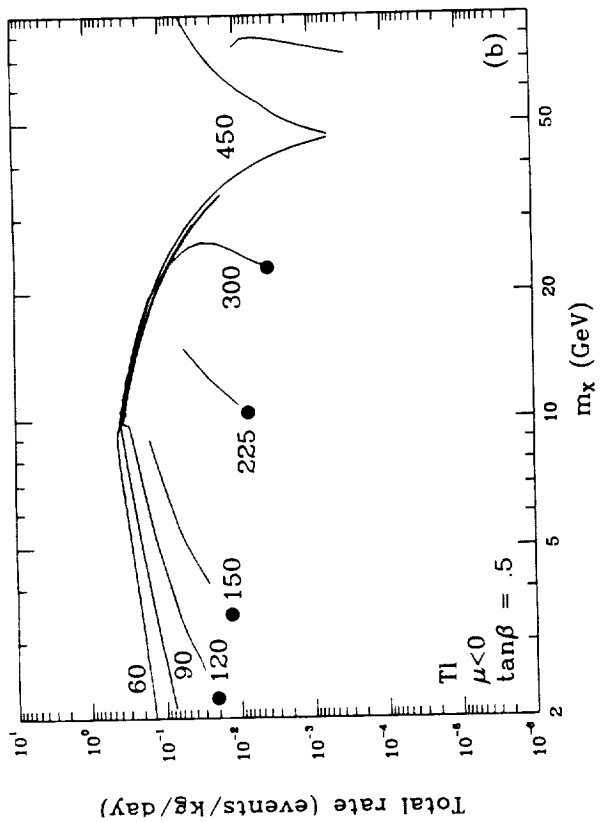

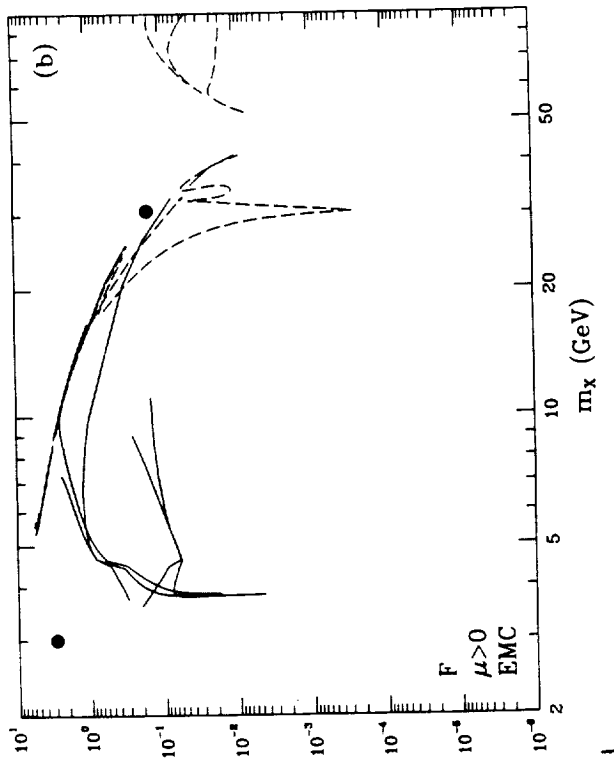

Fig. 4a, b

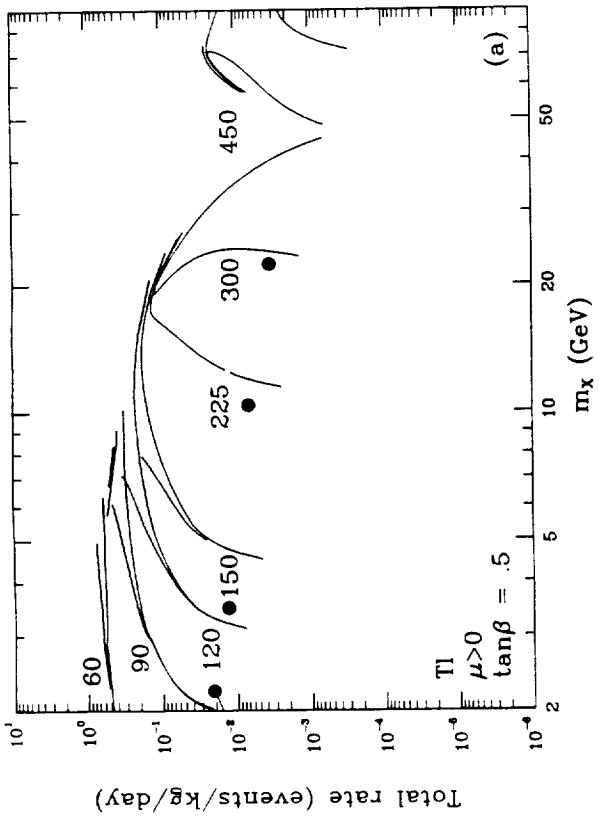

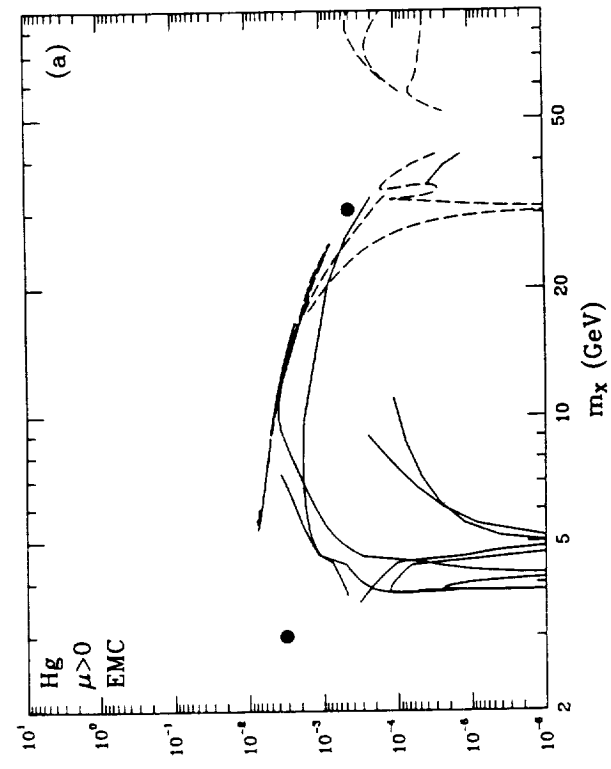

Fig. 5a, b